Chapter 3

Solution-State NMR of Lignins

John Ralph, Jane M. Marita, Sally A. Ralph, Ronald D. Hatfield, Fachuang Lu, Richard M. Ede, Junpeng Peng, Stéphane Quideau, Richard F. Helm John H. Grabber, Hoon Kim Gerardo Jimenez-Monteon, Yingsheng Zhang, Hans-J. G. Jung, Larry L. Landucci, John J. MacKay, Ron R. Sederoff, Clint Chapple, and Alain M. Boudet

Introduction

Despite the rather random and heterogeneous nature of isolated lignins, many of their intimate structural details are revealed by diagnostic NMR experiments. ^{13}C-NMR was recognized early-on as a high-resolution method for detailed structural characterization, aided by the almost exact agreement between chemical shifts of carbons in good low-molecular-mass model compounds and in the polymer *(1, 2).* Although this correspondence cannot generally be expected for proton NMR, lignin dimers and their counterpart units in the polymer also closely match proton NMR chemical shifts and coupling constants attesting to similar conformations of models and their polymeric counterparts *(3-5).* Lignin trimers provide slightly better data, and deliver revealing insight into the incredible stereochemical complexity of lignin oligomers and polymers and its impact on lignins' NMR spectra *(5).* Despite the broad featureless ID proton spectra, which have nevertheless allowed substantive interpretation *(6),* 2D spectra both homo- and heteronuclear, are informationally rich and strikingly useful. With modem NMR methods, there is the potential to elucidate structures without first preparing model compounds, although such models are still crucial for most studies, and for obtaining additional evidence of the identity of new structural features in the polymer.

Broadness of Proton Spectra

NMR practitioners know that increasing molecular weight broadens resonances due to reduced relaxation times. But lignins appear broader and more featureless than for example, comparably sized proteins. It is easily recognized that much of this broadness comes from the huge range of environments in the lignin polymer. Since

isolated lignins are polydisperse and have no regularly repeating macro-structures, each unit finds itself in a unique magnetic environment. But complexity in lignin extends far beyond the complexities caused by irregular bonding of one unit to the next. Even a β-O-4 ether homopolymer is a stereochemical nightmare *(5)*. In a lighthearted illustration, we demonstrated that for a regular 110-mer β-ether polymer the number of isomers (~10^{66}) approaches the number of atoms in the galaxy *(7)*. Therefore in any earthly quantity of a random β-ether polymer (with no other structural diversions), finding two identical molecules would be astronomically improbable. In a more realistic sense, this stereochemical complexity causes significant broadening due to the overlapping of NMR signals, as illustrated in Figure 1e (see p. 57). Even in a trimer, with 8 real (NMR-distinct) isomers *(5)*, the α-, β-, and γ-protons become complex, Figure 1c–d. Broadening of the lines in these spectra (which where sharpened for presentation and assignment purposes by careful anodization of the data), as would happen when the molecular weight is increased, would produce markedly broadened spectra It is not surprising then that proton spectra of lignins, Figure 1e, are so apparently featureless. Careful interpretation can reveal important details and, fortunately, the broadness is not an overbearing deterrent to producing valuable 2D correlations, as will be demonstrated.

The Sensitivity of Modem 2D Experiments

Two-dimensional spectra are acquired by taking sets of 1D spectra (with incremented delays between the spectra). It is often therefore assumed that 2D spectra must take much longer to acquire than 1D spectra. This has never been the case, since the signal-to-noise in 1D or 2D spectra depends on the *total* number of scans taken over the whole experiment. Even in the 'normally detected' C-H correlation experiments that now have a diminished role, the spectra can be acquired as quickly as normal 1D carbon spectra. The advent of inverse-detection (in which quantum mechanics provides a huge sensitivity gain when you excite and observe the sensitive proton instead of the carbon) and the enabling of commercial spectrometers to easily carry out these experiments, provided a welcome sensitivity enhancement for the difficult lignin polymers. The more recent advances of digital instrumentation, further improved signal to noise by digital oversampling, and application of strategically placed pulsed field gradients during acquisition allow spectra with fewer artifacts to be routinely acquired. [In our own case, we have only just acquired these latest capabilities so spectra included here cover non-digitail/non-gradient applications as well].

To illustrate the significance of these advances on informational content of NMR spectra, Figure 2 (see p. 89) compares 1D and 2D spectra obtained in under 4 minutes with reasonable amounts (80-100 mg) of a synthetic lignin (Figures 2a-c) and an

Figure 1: 1D spectra of sidechain regions of dimers, trimers, and lignin showing how lignins are broadened by their stereochemical complexity. Figures a) to d) are 600 MHz resolution-enhanced spectra of acetylated β -ether models: a) a free-phenolic dimer; b) etherified dimer; c) 4 of the 8 isomers of a trimer (etherified dimeric unit is *erythro);* d) the other 4 of the 8 isomers of a trimer (etherified dimeric unit is *threo).* e) Acetylated pine isolated lignin at 360 and 750 MHz.
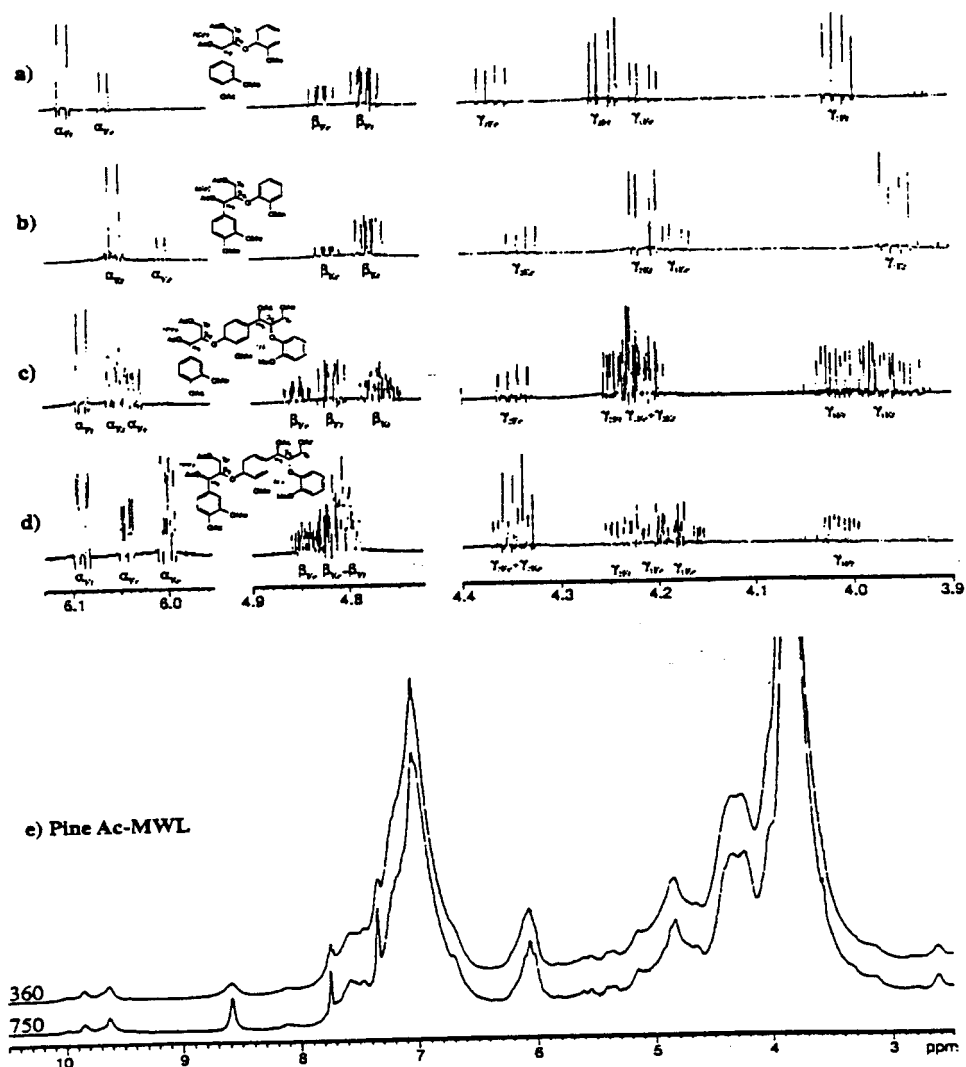
isolated softwood *(Pinus taeda)* milled wood lignin (Figures 2d-f) from a moderate-field (360 MHz) instrument. The 1D carbon spectra (2A 2d) in this time are minimally useful; spectrum 2d for the acetylated pine lignin shows methoxy and acetate methyl signals, but no more than a hint of aliphatic sidechain and aromatic carbons. In the same 4 minutes, the 2D gradient-selected HSQC spectra (Figures 2b, 2e, with expansions shown in Figures 2c and 29 provide diagnostic sidechain correlations for the major structural units. For the pine lignin, this supplies both proton and carbon chemical shift data that is unobtainable in similar time from 1D spectra (Figure 2d). Assignments of major peaks are made using labels for the muctures as defined in Figure 2g. Better quality spectra (acquired over longer periods) for both samples appear later, with more complete assignments.

A Problem with (Early) Inverse Heteronuclear Experiments

The major problems in the early inverse experiments, particukrly HMBC *(8)* and HMQC *(9),* were related to T_1-noise artifacts which were particularly obstructive in lignins due to the intense methoxy signals. These artifacts are caused primarily from pulsing each scan before complete relaxation to the equilibrium state; so-called rapid-pulsing is favored however for improving signal-to-noise in a given experiment time. Methoxy resonances are relatively sharp and intense in both the proton domain (where the 3-6 methoxy protons per monolignol unit cause the methoxy peak to dominate proton spectra) and the carbon domain (where the narrow methoxy chemical shift range causes a similarly dominant methoxy carbon peak). The result in proton-detected 2D spectra is an almost complete obliteration of information from protons resonating near the methoxy group. Although this problem can now be overcome by the use of pulsed field gradients on appropriately configured newer instruments (see later), an attractive solution for synthetic lignins is labeling that makes the methoxy group NMR-invisible. This is achieved by use of monolignols synthesized to contain deuterated and ^{13}C-depleted methoxy groups *(10).*

As shown in Figure 3 (see p. 90), a variety of 2D NMR spectra of a synthetic lignin produced with NMR-invisible methoxy groups (right) from labeled coniferyl alcohol are markedly superior to those from an equivalent lignin made from normal coniferyl alcohol (left). The spectra are: a) and e) HMQC (non-gradient); b) and f) DEPT-HMQC with a $\pi/3$ editing pulse (CH's up, CH_3's and CH_2's down); c) and g) HMQC-TOCSY (non-gradient, 80 ms TOCSY mixing time); d) and h) HMBC (100 ms long-range [13]C-^{1}H coupling delay). Dashed lines are negative contours. Assignment colors and letters are the same as in Figure 2g: on HMQCs, the structure (a-E-X) followed (smaller size) by the sidechain C-H pair (e.g. Bβ is the structure B Cβ/Hβ correlation); on HMQC-TOCSYs, the structure is followed by the carbon excited in the HMQC part followed by the proton from the TOCSY part (e.g. B $\beta\alpha$ is the structure B Cβ/Hα

correlation); on HMBCs, the structure is followed by the carbon followed by the coupled proton within 3-bonds *(e.g.* Bβα is the structure B Cβ/Hα long-range correlation). The spectra also illustrate the value of spectral editing in 2D NMR experiments that has not yet attracted much attention from lignin chemists. The DEPT-HMQC *(11)* experiments, can aid in assignment by inverting (for example) -CH$_2$ resonances (Figures 3b and 3f). The HMQC-TOCSY *(12)* experiment (Figures 3d and 3h) is still underutilized in plant cell wall research. It provides beautifully linked correlations that greatly facilitate rapid assignment of lignin spectra, particularly in the sidechain region.

The freedom from artifacts in these "methoxy-less" lignin spectra allows more detailed assignments to be made; all of the major subunits are assigned in selected spectra of Figure 3. Such assignments aid in the characterization of isolated plant lignins.

Advantages of Higher Magnetic Fields

The advantages to spectral dispersion and signal-to-noise of going to increasingly higher magnetic field strengths are well known. Above about 250-300 MHz, higher field strengths do not however produce carbon spectra with improved resolution or dispersion the dispersion gains are almost exactly offset by added line broadening. A carbon spectrum run on a 360 MHz instrument is almost indistinguishable from one run on a 750 MHz instrument except for signal-to-noise improvements. Fortunately, proton spectra do gain significantly in spectral dispersion and higher field is invaluable for proton ID experiments as well as any 2D experiment with proton data in one or more dimensions (H-H correlation, J-resolved, C-H correlations). Sensitivity is also markedly improved at higher field strengths.

Completely unfair comparisons of ^{13}C-enriched ryegrass lignin HMBC spectra taken on 360 MHz (non-digital) and 750 MHz (digital, gradients) instruments shows the increased resolution achievable, Figure 4 . The 360 MHz HMBC was run on a traditional (non-digital, no gradients) system using a 10 mm broadband probe of normal geometry; 80 ms long-range coupling delay. The 750 MHz gradient-selected HMBC spectrum used about one third the amount of mateiral (60 mg) for half the time in a 5 mm inverse probe; 100 ms long-range coupling delay. Figures c) to e) are expansions of a small section of the α-proton correlations in β-ether units A, showing the improved resolution and sensitivity in the 750 MHz spectrum: c) expansion of 360 MHz spectrum; d) expansion of 750 MHz spectrum; e) same expansion as d) but with contours set lower so that more minor correlation peaks can be seen (above the noise level). The only problem is that these beautiful spectra now have more peaks that need interpreting!

Figure 4: Comparisions of ryegrass lignin HMBC spectra at 360 and 750 MHz.
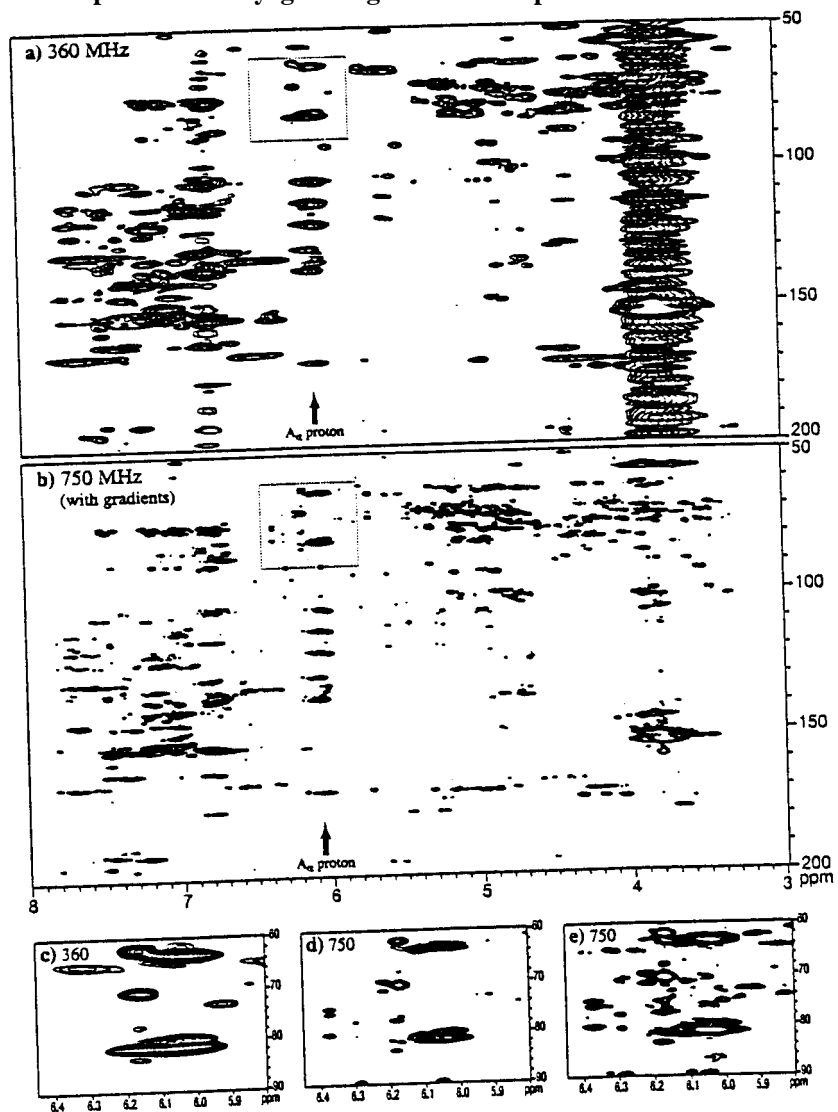
Important Classes of 2D spectra

From the many hundreds of NMR experiments, a few have filtered out as representatives of various classes of experiment. Original references to experiments mentioned here can be found in modem books on NMR; the book 100 *and More Basic NMR Experiments (13)* is a good starting place for getting an overview of the experiment as well as hints on parameter selection and basic processing.

a) Homonuclear Correlation (COSY and TOCSY class)

As noted above, proton-proton 2D experiments are extraordinarily valuable despite the poor appearance of ID proton spectra. Broadness *per se* is not a significant deterrent in spectra which are taken at much lower resolution than 1D spectra. While COSY type experiments are valuable (14, 15), the extra correlations provided by TOCSY experiments makes them particularly attractive.

Interpreted TOCSY spectra are given in Figure 5 (seep. 91). TOCSY spectra are of a) an acetylated coniferyl alcohol synthetic lignin (DHP) and b) an acetylated *Pinus taeda* lignin. In the pine lignin the near absence of products from monolignol coupling is particularly apparent from minor contours corresponding to endgroups X and resinols C. Note also the virtual absence of α,β-diethers E. One type of dihydroconiferyl alcohol product Y appears in the pine lignin, but two different products Y are in the DHP. This will be discussed in more detail with Figure 21 (see p. 102). Color/structure assignments are as in Figure 2g.

In such TOCSY spectra, the mixing time determines the relative intensity of the various contours; mixing times of 80-120 ms are typically used. A short mixing time (10-30 ms) yields essentially COSY-type spectra where protons see only their directly coupled neighbors. The TOCSY (also called HOHOHA) experiments have some advantages over COSY and long-range COSY experiments for lignins *(16)* — during the mixing time, relaxation is less significant and TOCSY spectra are less sensitive to the initial state of the magnetization (meaning that pulsing can be faster). TOCSY spectra have been reported often *(3, 4, 14, 16 - 25),* and have been valuable in finding minor structures in lignins *(3).* In the Applications section, we present TOCSY evidence for a new aryl isochroman structure resulting from β-1-radical coupling in softwood lignins. The long-range variant of the COSY experiment has found particular use in low-molecular mass lignin models and lignans *(26).* The older relayed coherence transfer experiments can provide similar data and were useful for assigning trimeric lignin model β-ether isomers *(5).*

b) Homonuclear J-Resolved

J-resolved experiments separate chemical shift in the acquired dimension and proton-proton coupling in the second dimension, Figure 6 (see p. 91). Refocusing of relaxation effects from magnetic field inhomogeneity is an asset when seeking small (long-range) coupling constants in model compounds, but J-resolved experiments are not widely used because of second-order artifacts that arise from tightly coupled protons. Higher magnetic fields can often simplify these spectra since tight coupling, where two distinct coupled protons have chemical shifts (in Hz) that differ by less than ~10J (where J is the coupling constant in Hz), becomes less frequent; two protons which are only 20 Hz apart at 200 MHz are 75 Hz apart at 750 MHz, for example. For lignins J-resolved experiments have revealed useful information. The first-order α-protons in β-ether units of acetylated lignins allow *threo-* and *erythro-* isomers to be distinguished based on a combination of their chemical shifts and coupling constants *(15)*. Figure 6b shows proton J-resolved spectra of a) an acetylated coniferyl alcohol DHP and b) an acetylated pine isolated lignin in acetone-d_6. The expansion in Figure 6b shows how the *threo-* and *erythro-*isomers are resolved. The *three-isomers also* resolved into etherified (e) and free-phenolic (f) components. In CDCl$_3$, there is further resolution of etherified vs non-etherified β-ether units *(15)*. Color/structure assignments are as in Figure 2g.

c) Through-space Homonuclear correlation NOESY/ROESY

NOESY or ROESY spectra correlate protons that are close to each other in space (rather than through-bond). The magnitude of the interaction falls off with the 6th power of the distance between the twvo protons, so such interactions are diagnostic for inter-proton distances of less than about 5 Å. They are consequently preeminent experiments for deducing 3D solution-state conformations for proteins — the NOESY data provide sufficient numbers of distance constraints to allow constrained molecular modeling to produce essentially unambiguous 3D structures. However, due to the absence of regularly repeating macro-structures in lignins and perhaps to their rather linear nature with little chain folding, correlations are few and limited to intra-unit responses, and therefore provide little confirmational insight. The major correlations seen are between the methoxy protons and the aromatic 2-proton in guaiacyl units or the 2/6-protons in syringyl units, and between sidechain protons (Hα Hβ and Hγ) and aromatic protons (H2 and H6) of the same unit *(16, 19)*. Perhaps the depressingly unrevealing NOESY/ROESY spectra provide the best evidence that milled wood lignins and other solvent-extractable lignins have little in the way of structural regularity, a conclusion also arrived at by noting the complexity of 1D ^{13}C-NMR spectra of lignins. Even in a highly syringyl-rich lignin where long arrays of β-O-4-coupled units exist, such as in birch *(19)* or the bast fibers of kenaf *(22),* no useful interunit correlations are seen. On low molecular mass lignin models and lignans, the NOESY experiment is of course valuable for identifying isomers and

for the confirmational data it provides. For example, isomers of the various 8-β - coupling products from ferulates and coniferyl alcohol can be nicely distinguished by NOESY and long-range COSY experiments *(26)*.

d) Inverse C-H correlation (HMQC-class)
By far the most useful experiments are those providing correlations between protons and carbons in two dimensions. Extra "apparent" resolution is gained far exceeding anything that can be achieved in 1D spectra with today's field strengths. Overlapping protons that are attached to carbons with different shifts are pulled out by those carbon shift differences, whereas overlapping carbons may be pulled out by their attachment to protons with differing chemical shifts.

So great are the advantages of the so-called "inverse-detected" experiments (where the proton dimension is acquired, rather than the carbon one) that-little use is now made of the older normal-mode experiments (carbon dimension acquired) except on older instruments. As noted earlier and in Figure 2 (seep. 89), satisfactory HMQC (or HSQC) spectra can be run in as little as 4 minutes with gradient selection, or about 16 minutes without. Longer acquisitions obviously still give valuable signal-to-noise improvements and consequent interpretability enhancements, so longer experiments are still recommended for detailed work.

HSQC or HMQC spectra. Figure 7 (see p. 92) shows gradient-HSQC *(27-29)* spectra of several lignins, with interpretation of major structural units A-E, X-Y. An HSQC contour implies that a proton at the proton frequency of the contour (x-axis) is directly attached to a carbon at the carbon frequency of the contour (y-axis). Note the dominance of β-ether structures A in all but the synthetic lignin. The samples are: a) synthetic ("methoxy-less" — see Figure 3) coniferyl alcohol DHP; b) soluble lignin from *Pinus taeda; c)* soluble lignin from a *Tainung* kenaf *(22);* d) lignin from the hardwood, aspen; e) soluble lignin from ryegrass, ^{13}C-enriched *(39);* a lignin (solubilize in 69% yield) from mature maize (corn) stems *(32).* Color/structure assignments are as in Figure 2g. Assignments are initially made from the model compound data which have been accumulated over the years in 1D experiments. A repository of such data is available via the internet *(30).* The availability of an assigned spectrum for example the clean synthetic lignin spectrum in Figure 7a, allows major structures in other spectra to be rapidly assigned. HMQC or HSQC spectra of lignins have been well reported *(3, 14, 16, 18, 19, 31, 32).*

The HMQC/HSQC experiments have been valuable in assigning major structures of course, and have been indispensable in identifying new and minor units. The clear identification of dibenzodioxocins D as major new structures in lignins has been a significant finding *(33-35).* In acetylated lignins, they are readily identified by unique

and often well-resolved correlations in HMQC/HSQC spectra, Figure 7 (see p. 92, and also Figure 24, p. 104). It is worth stressing that evidence provided by 2D NMR is far more diagnostic than 1D data purely because of the simultaneous constraints that are revealed in the data. Thus, the observation that there is a proton at 4.9 ppm directly attached to a carbon at 84.4 ppm and a proton at 4.1 ppm attached to a carbon at 82.5 ppm is more revealing than just observing two new carbons at 84.4 and 82.5 ppm in 1D spectra Further details regarding dibenzodioxocins and the tentative identification of a new β-1 pathway are illustrated in the Applications section.

Although 2D correlative spectra have the advantage over 1D of providing at least two pieces of simultaneous data, overlap and confusion can still occur in 2D. One pitfall in HMQC and HSQC spectra is found with structures E (α, β-diaryl ethers) and F (α-keto-β-aryl ethers). The a-proton/carbon contour in E is in almost exactly the same region and the β-proton/carbon contour in F, at *ca* 5.6/81 ppm. β-Keto units occur mainly in syringyl-rich isolated lignins, and maybe produced during ball-milling and lignin isolation. Distinguishing the two components is best made in HMBC spectra where in guaiacyl α-ethers, for example, H-E $_\alpha$ (5.6 ppm) correlates with carbons γ (63.5), β (81.5), 1 (137.5), 2 (112.3), 6 (120.0), and 4 (147.5) of the next unit— see later in Figure 9 (see p. 93). In contrast, in units F, H-F$_\beta$ (5.6 ppm) correlates with carbons γ (64.5), and diagnostically α (194.8). Confirming structural assignments from all obtainable data is therefore recommended.

As noted in the section above entided "A problem with (early) inverse heteronuclear experiments" and in Figure 3 (see p. 90), multiplicity editing in 2D NMR is possible via for example, DEPT-HMQC *(11)* experiments. A 60° editing pulse yields spectra with CH contours positive, CH$_3$'s and CH$_2$'s negative, Figure 3b,f; a 180° editing pulse gives CH's and CH$_3$'s positive and CH$_2$'s negative, and is therefore analogous to the 1D DEPT sequence with a 135° editing pulse. Although useful and potentially cleaner spectra can be obtained this way, these sequences have been little utilized in lignin work to date.

HMQC-TOCSY or HSQC-TOCSY spectra. An experiment enjoying more widespread utilization is the 2D HMQC-TOCSY experiment *(12)* or its relative, HSQC-TOCSY *(36)*. Although less sensitive than their HMQC/HSQC counterparts (because of the extra correlations for each proton and carbon), the redundancy in information and the clear identification of coupling networks is enormously useful *(19, 20, 22-24)*. The assignments in HMQC/HSQC spectra, Figure 7 (see p. 92), must be made with good knowledge of both carbon and proton chemical shifts for each structural type. In contrast, in HMQC-TOCSY spectrra, Figure 8 (see p. 93), a knowledge of rough proton shifts allows very rapid identification of units because of the useful redundancy in the data. Knowing that acetylated β-ether units have α-

protons at ~6 ppm, β-protons at ~5 ppm, and γ-protons between 4 and 4.6 ppm, allows the blue contours to readily be assigned to β-ether structures A, for example. It is further easy to see which carbons are in the same structure — simply look for matching sets of correlations in the proton dimension. The DHP spectrum 8a) is particularly useful because all of the important possible inter-unit structures are present in a single sample. Note that the syringyl-rich kenaf lignin is exceptionally rich in β-either units A. Color/structure assignments are as in Figure 2g. Because of the differences in proton coupling constants and the ability to transfer magnetization around the coupling network the proton correlations for each carbon (or vita versa) will not all have the same intensity and some may even be absent, but it is very easy to recognize that all the blue peaks (β -ether structure A) belong together as do all the green peaks (phenylcoumaran structure B), etc. The simple interpretability of the sidechain region of 2D HMQC-TOCSY spectra and the valuable redundancy of correlation peaks make this experiment one of the most useful.

The HMQC-TOCSY experiment was the key to rapid identification of novel dihydroconiferyl alcohol units present in a mutant pine lignin, and tyramine units in genetically altered tobacco lignins, as described in the Applications section. Selecting appropriate mixing times for this experiment is dealt with in the "Identification of new structures" section.

e) Inverse long-range C-H correlation (HMBC-class)
Whereas the HMQC/HSQC-type spectra are valuable for their direct attachment information and because of the" apparent extra dispersion they provide over ID spectra, long-range experiments provide enormously valuable connectivity data Two- and 3-bond C-H coupling constants are in the 2-15 Hz range, and HMBC *(8)* experiments are typically set with coupling evolution times of 80-120 ms, corresponding to coupling constants of 4-6 Hz. It is possible to miss correlations because they may be twice the set value, for example (the response is a sine curve centered about 1/2J). In some circumstances it maybe appropriate to run spectra with varying evolution times to allow for all correlations to become visible, but as with the HMQC-TOCSY experiment, the useful redundancy of data often makes this unnecessary. If a given correlation from a particular structure is required the experiment can be easily optimized for that correlation by appropriately choosing the coupling evolution delay as $0.5/J_{LRCH}$, using the long-range coupling constant of interest. For example, to see ferulate arabinose attachments, we chose 110 ms corresponding to the measured $^{3}J_{C-O-C-H}$ of 4.5 Hz *(37)*. What must be kept in mind with polymeric lignin samples, however, is that the longer this delay, the less intensity the spectrum will have due to rapid relaxation losses. Obviously if a (proton) FID of the lignin is reduce-d to the noise level in 100 ms, running an HMBC experiment incorporating a 100 ms delay will produce nothing. Some isolated lignins,

especially those prepared by steel ball-milling, can have very short relaxation times that can often be improved by EDTA washing the lignin *(32)*. Acetylated samples can readily be EDTA-washed in an extraction step, and this is almost always worthwhile *(38)*.

A single partially-assigned HMBC spectrum from the synthetic lignin (acetylated) sample of previous figures is shown in Figure 9 (see p. 93). Color/structure assignments are as in Figure 2g. Note the beautiful proton-α correlations with carbons β, γ, 1, 2 and 6 in the β-ether units A. Also note however that β-proton correlations are sparse; this is because proton-proton coupling is more extensive and more varied for the β-protons.

Applications of HMBC experiments to lignins have been documented *(14, 18, 20, 21, 31, 32, 37, 39)*. The enormous power of this experiment can be seen in applications (below) which show unambiguously how *p*-coumarates and acetates are attached to γ-positions of lignins, how syringyl and guaiacyl structures are distinguished, and reveal how ferulates are incorporated into natural and synthetic lignins (effecting lignin polysaccharides cross-linking). The information rivals that from the diagnostic [13]C-^{13}C-correlated INADEQUATE experiments, but HMBC spectra are obtained with significantly higher sensitivity and allow correlations to be made over several bonds (and therefore through oxygen and nitrogen, for example) which the INADEQUATE experiments cannot.

f) Carbon-carbon correlation, INADEQUATE experiments

INADEQUATE experiments *(40-42)* correlate two neighboring ^{13}C-resonances and operate through direct [13]C-^{13}C coupling so are consequently low-sensitivity experiments. Uniform ^{13}C-labeling at the 10-15% level provides an enormous sensitivity increase while keeping carbon ID spectra relatively free of homonuclear coupling peaks and long-range-coupling effects minimal. Many versions of the experiment exist, including newer more sensitive implementations with INEPT-type transfer and with gradients. Some of these implementations only provide connectivity for protonated carbons, however. A version providing symmetric COSY-like correlations *(42)* was used in the only previously published lignin spectra of this type. A series of papers *(43-45)* illustrated the connectivity available for the major units in a uniformly ^{13}C-enriched poplar lignin *(46)*.

Figure 10 is from a symmetrical 2D INADEQUATE spectrum of a ^{13}C-enriched ryegrass lignin (that contained significant polysaccharides components). The plot shows just the sidechain region. Although there are many improved INADEQUATE methods, the symmetrical presentation of this particular experiment, like a ^{1}H-^{1}H COSY spectrum, is particularly easy to interpret. Basically, it reveals that carbon-a is

linked to carbon-β which is linked to carbon-γ. This kind of connectivity information helps track through the resonances from a given structural unit. Structures B and C are traced out in the figure. Resonances from A-units are more complex and are complicated by polysaccharides impurities-they are not traced out here. Connectivity information can be less directly gained by using long-range C-H correlation, in the more sensitive HMBC experiment.

Figure 10: Partial INADEQUATE spectrum showing just the sidechain region, from a ^{13}C-enriched ryegrass isolated lignin that contained substantial polysaccharides components.
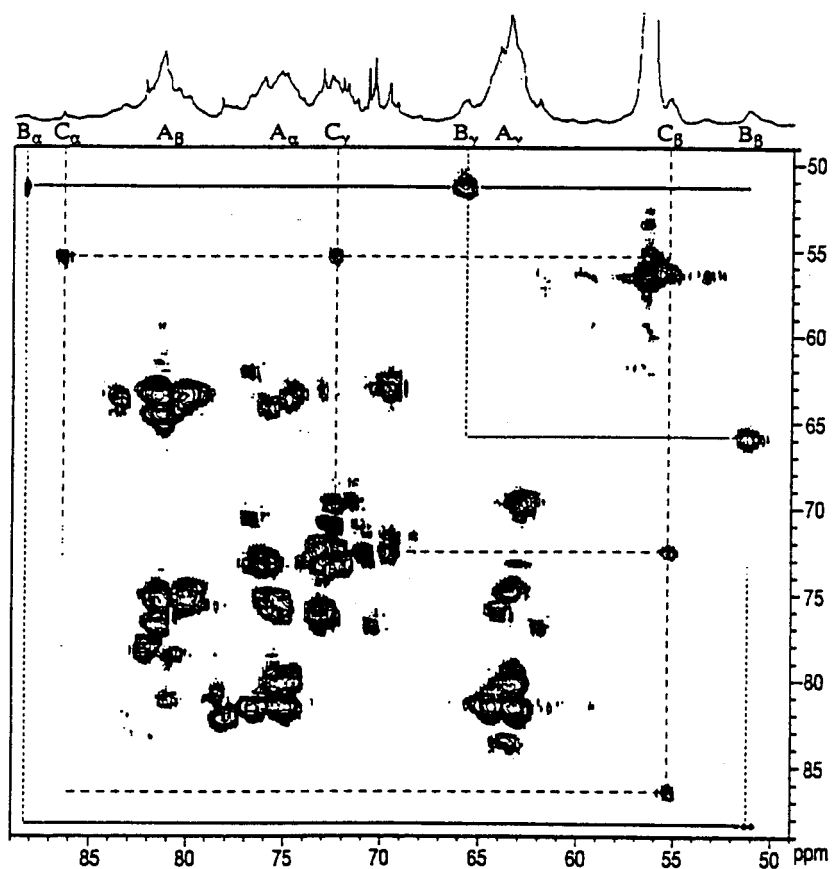
g) Higher-dimensional spectra (3D, 4D, ...)

NMR is not limited to 1- and 2-dimensions. Three-dimensional experiments are now commonplace, and 4D-, 5D-, and higher-D-experiments have been applied to labeled proteins. Much of the value of these experiments comes from the further dispersion realized by correlating over the additional dimensions. This is particulary valuable in proteins where ^{13}C, ^{1}H, and ^{15}N dimensions are available. For uniformly ^{13}C-enriched lignins, the 3D HMQC-TOCSY experiment (with one ^{13}C and two ^{1}H axes) has been applied with some success *(47, 48).* The increased complexity and data size, and the reduced resolution provide less than compelling advantages over 2D experiments, although their value is becoming appreciated. The expectation that 3D experiments necessarily are more time demanding again overlooks the fact that signal-to-noise is gained on the total number of scans in the entire experiment. Although labeled materials facilitate 3D (as well as 1D and 2D) experiments, valuable spectra from unlabeled materials are readily obtained.

Figure 11a (see p. 94) shows a 3D-HMQC-TOCSY experiment (100 ms TOSCY) of the "methoxy-less" lignin (seen in Figure 3, p. 90), with natural ^{13}C-abundance. In a weekend, this 3D experiment provides ample sensitivity for a synthetic lignin. The spectrum is obtained without applying any of the sensitivity- or resolution-enhancement treatments such as linear prediction in the 3D processing. The 3D data-set is rather pretty but spectacularly useless until 2D projections or slices are made for viewing and plotting. More informative 2D sub-spectra for the prominent structures in lignins are shown in Figures 11b-d. Note how "clean" most of these sub-spectra are — a result of dispersion into a third dimension. The slices show b) a 2D HMQC-TOCSY (as seen previously in Figure 8a) for comparison with the following; c) the first 2D slice in the F_1-F_3 plane is essentially the same as the 2D experiment in b) — differences with this particular experiment are the residual l-bond ^{13}C-^{1}H coupling between the excited proton-carbon pair (see below); d) F_1-F_3 slices at various proton frequencies (in F_2) showing the beautiful resolution of the major units in HMQC-TOCSY-type sub-spectra e) two F_2-F_3 slices to show the TOCSY-type data available at selected carbon frequencies (in F_1).

The particular pulse program used for Figure 11a-e (Bruker's "invbm13d") is not a gradient experiment and has two features requiring comment. Firstly, the sequence, like its 2D-HMQC-TOCSY counterpart ("invbmltp") uses a pre-excitation BIRD sequence *(9)* to reduce the unwanted intensity from protons attached to NMR-inactive ^{12}C. The BIRD sequence takes about one third of the experimental time; no real data are collected during this time. The other 'feature' is that the directly bonded C-H pair that is excited in the HMQC portion of the expexirment retains its $^{1}J_{C-H}$ coupling (~140 Hz). This is illustrated with the slices that are plotted in Figures 11c-e.

More modem versions using gradient selection decrease the time requirement. A more efficient TOCSY-HSQC experiment has been implemented by Bruker ("mleviietf3gs3d" which can be modified to a two-channel version, "mleviietgs3d") and provides beautiful HSQC sub-spectra in the F_2F_3 plane and TOCSY sub-spectra in F_1-F_3. We have run this 3D experiment on the same synthetic lignin sample in as little as 6h.

Figure 11f-k: Gradient-edited 3D-TOCSY-HSQC experiment (100 ms TOCSY) on a synthetic DHP (the same sample as Figure 11 a-e), at natural abundance; F_3-F_2 slices.
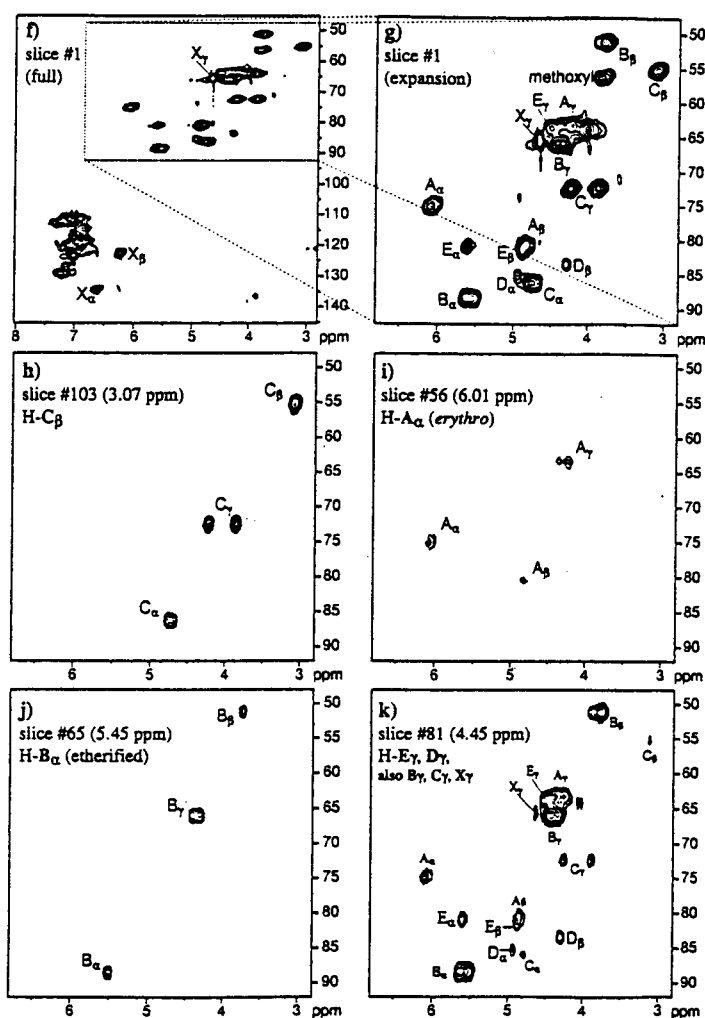
Figure 11f-k shows F_3-F_2 slices from the gradient-edited 3D-TOCSY-HSQC experiment (100 ms TOCSY, on the same sample as Figure 11a-e); the 3D plot is not shown. Structure assignments are as in Figure 2g. The various plots are: f) the first 2D slice in the F_2-F_3 plane which is essentially the same as a 2D HSQC experiment — compare Figure 2b or Figure 7a; g) expansion of the major sidechain region of slice 1; h) slice through $\delta_H = 3.07$ (H_β of etherified C units) showing a pure HSQC spectrum of the sidechain of etherified resinol structures C; i) slice through $\delta_H = 6.01$ (H_α of *erythro* -A units) showing a pure HSQC spectrum of the sidechain of *erythro*-β-ether structures A; j) slice through $\delta_H = 5.45$ (H_α of etherified B units) showing a pure HSQC spectrum of the sidechain of etherified phenylcoumaran structures B; k) slice through $\delta_H = 4.45$ (H_γ of structures A, B, C, D, E, and X all overlap) showing composite HSQC spectra of the sidechains of all of these structures.

Figures 11h-j show how, if a proton chemical shift is unique, it is possible to observe HSQC spectral planes that are purely from a single substructure in lignin (as seen for structures A, B, and C). Where protons are not unique, HSQC spectra of several units are obtained, such as is the case at 4.45 ppm, where γ-protons of substructures A, B, C, D, E and X all resonate, Figure 11k.

The following brief introduction is provided for those new to the 3D experience. The 3D HMQC-TOCSY experiment, Figures 11a-e (see p. 94) is acquired with three orthogonal dimensions, labeled F_1, F_2 and F_3. The acquired dimension is F_3 and, for sensitivity reasons, is proton. F_2 is also proton, and F_1 is carbon. Since this is an HMQC-TOCSY experiment, a 2D F_1F_3 plane is basically a 2D ^{13}C-^{1}H HMQC-TOCSY spectrum at a given proton chemical shift (defined by the distance along the proton F_2 axis). Thus, *e.g.* Figure 11d(vii), at the plane through the H-α proton frequency of phenylcoumaran B structures, we see C-α (~88.5 ppm) correlating (in TOCSY fashion) with the H-α (~5.6 ppm, split by $^1J_{C\alpha\text{-}H\alpha}$), H-β (3.76 ppm), and H−γ (~4.4 ppm). Similarly, a 2D F_2F_3 plane is basically a 2D ^{1}H-^{1}H TOCSY spectrum at a given carbon chemical shift (defined by the distance along the carbon F_1 axis). Thus, *e.g.* Figure 11e(i), at the plane through the C-γ carbon frequency of phenylcoumaran B structures, we see H-α (~5.6 ppm) correlating (in TOCSY fashion) with the H-β (3.76 ppm), and H-γ s (~4.4 ppm, split by $^1JC_\gamma\text{-}H_\gamma$). Although the profile looks similar, note that the vertical axis of the 2D sub-plot is ^{13}C for Figures 11d and ^{1}H for Figures 11e. The first plane in either dimension is, like in a 2D experiment, very much like a projection of all resonances onto that plane (but with lower signal-to-noise since it represents only a single plane). Therefore, Figure 11c, the 2D F_1F_3 first plane, is similar to the 2D HSQC-TOCSY spectrum Figure, 11b (seen previously in Figure 8, p. 93). [Unfortunately, we acquired one nasty artifact at

about 70 ppm by having the acquired dimension end right on a signal - we were lucky that no other peaks of interest came at a carbon chemical shift of 70 ppm!]

The 3D gradient-selected TOCSY-HSQC spectrum Figure 11f-k (see p. 69, 3D plot not shown) is understood similarly. In this case, the acquired dimension is again F_3 (proton), but this time F_2 is carbon and F_1 is proton. F_2-F_3 planes are basically 2D ^{13}C-^1H HSQC spectra The proton shift (on F_1) of the F_2-F_3 plane can be considered as the initially excited proton, which then transfers magnetization to all of the protons in its coupling network. For example, Figure 11i an F_1 proton shift of 6.01 corresponds to the α-sidechain proton of β-aryl ether units A (in fact just the *erythro*-isomers); that proton is in the same coupling network as the β- and the two γ-protons on the same sidechain. During the subsequent HSQC step, each of those sidechain protons correlates with their respective attached carbons. The result in the ideal case is a clean HSQC spectrum of one single unit type, *e.g.* Figures 11h-j (see p. 69) for structures C, A, and B respectively. Such clean spectra derived from individual units in a complex polymer like lignin are an obvious asset for identifying structures— the early lignin structure pioneers could certainly have benefited from such a powerful diagnostic tool. In a similar fashion to F_2-F_3 slices in the non-gradient HMQC-TOCSY experiment described above (Figure 11e), The F_1-F_3 planes show TOCSY correlations for the proton attached to the carbon at the F_2-frequency of the plane with all of the other protons in the coupling network of that attached proton (not shown).

Processing

Processing of 2D NMR spectra is a huge subject that can scarcely be touched here. All of the spectra shown in this chapter were processed by entirely conventional anodization means, without using linear prediction or other sensitivity- and resolution-enhancing methods which might be valuable. It is important to note that application of default anodization methods is rarely optimal. For example, the sine and sine-squared apodizations applied in the processing of most experiments can almost always be improved by the application of Gaussian apodizations. While this may not be particularly important for small molecules where sensitivity abounds, taking the time to select suitable anodization in lignin spectra can make or break an experiment. Fortunately, most modern instruments have software that allows real time manipulation of anodization of at least 1D slices. As an example, the HMBC experiment is an echo type experiment where most of the intensity in any row (the first row is usually chosen for inspection) will be maximal at the chosen J-coupling delay, say 100 ms. Therefore, blindly applying a Q0 (sinebell-squared) anodization could completely miss that maximum and not reflect the shape of the FID. For example, if the acquisition time was 300 ms, then the maximum in the data will be

only one third of the way along the FID, not half way (as assumed by the Q0 apodization). Using Gaussian apodization, you can closely match the FID in both shape and position of the maximum. (For example, Gaussian anodization with a line broadening of ~-30 Hz and a GB of 0.33 would be superior in the above example). More extensive treatises on processing of NMR spectra are available *(49-51).*

Applications

The following sections provide examples largely from our own laboratories of the application of NMR methods to solve structural and mechanistic problems related to lignin, lignification, and cell wall cross-linking. It is hoped to illustrate not only the use of various NMR techniques to solve such structural problems, but the enormous power of NMR to provide such structural insights. Although complementary techniques and other analytical instrumentation are obvious assets in this type of research, it is NMR that is able to provide some of the most unambiguous and diagnostic insights.

Natural lignin esters

Esters of various types are found in certain lignins. Hardwoods contain acetate groups reportedly on lignins *(52),* and all grasses contain varying levels of *p*-coumarates *(21, 32, 53-60).* Some plants also contain *p*-hydroxybenzoates on lignin *(61-63).* NMR is able not only to confirm such lignin acylation, but provides unambiguous regiochemical elucidation — the regiochemistry (or site of attachment) provides biochemical insights.

Acetates. Acetates have not been seriously addressed, in part due to the common practice of immediately acetylating lignins to improve their solubility and NMR characteristics. The recent report *(22)* of high levels of acetate on kenaf bast fiber lignins has been unambiguously validated by several unrelated experimental methods and on several kenaf clones *(64).* Figure 12 (see p. 95) shows the 1D and 2D spectra identifying such acetylation and establishing that the acetates are primarily at the γ-sidechain position. Acetates will migrate from the γ- to the α-position *(65),* so strict regiochemistry is not expected. Experiments based on the "DFRC" (Derivatization Followed by Reductive Cleavage) degradative method confirm the regiochemistry and further reveal that acetates are almost entirely on syringyl units *(64).* Such products may implicate the biosynthesis of sinapyl γ-acetate as a precursor of kenaf lignin. The functional role of such high levels of acetates in kenaf lignins awaits explanation. Although present at much lower levels, acetates on the γ-position have been confirmed in aspen by a modified DFRC analysis *(64).* Detailed NMR studies elucidating the nature of these minor acetate levels have not been carried out.

Figure 12 (see p. 95) shows spectra from *Tuinung kenaf* isolated lignin. a) The lignin was isolated from the bast fibers, not the core *(22);* b) 1D ^{13}C-NMR spectrum of acetylated kenaf lignin shows it to be particularly syringyl-rich c) 1D ^{13}C-NMR spectrum of unacaylated kenaf shows that the lignin bears its own natural acetates; d) a gradient HSQC spectrum of unacetylated kenaf lignin shows clear acylation at the γ-position; a low amount of α-acylation comes from natural acetyl group migration; e) a gradient HSQC-TOCSY (100 ms) spectrum again shows the clearly acetylated γ-position. Colors do not relate to those in other figures.

p-Coumarates on grasses. All grasses contain lignins that are partially acylated by *p*-coumarate. The functional role has not been fully elucidated although some excellent theories are now emerging *(66-68).* Regiochemistry of *p*-coumarate attachment is again an important consideration in understanding the mechanism of its incorporation. Acylation at the α-position implicates attack of *p*-coumaric acids on quinone methides, intermediates following radical coupling reactions. As has been pointed out *(21, 37),* such (non-enzymatically catalyzed) chemical reactions are difficult for the plant to control as the quinone methide has a number of competing substrates, including water, for addition reactions. Acylation at the γ-position may again implicate transferase enzymes in the creation of pre-formed hydroxycinnamyl *p*-coumarates which can subsequently be incorporated into lignins via radical coupling reactions *(21, 32, 69).* The two reaction pathways are vastly different biochemically, implicate different enzymes, and have different temporal and spatial requirements.

Early studies on bamboo using *W* to distinguish *a-* from γ-esters suggested mixed regiochemistry acylation was estimated at 80% γ to 20% α *(69).* Our findings *(70)* that *p*-coumarate did not migrate (unlike acetate *(6.5))* made such a dichotomy troubling — it implied that *p*-coumarates were attached to lignins by two completely divergent mechanisms. NMR methods were sought to determine *p*-coumarate regiochemistry.

As seen from Figure 13 (see p. 96), the elucidation of attachment regiochemistry by NMR is elegant and unambiguous *(32).* Spectra a) to f) are HMQCS: a) a *threo-* β *ether-* g-*p*-coumarate model; b) an *erythro-* β *-ether-* g-*p*-cournarate model; c) the β-5 dehydrodiconiferyl alcohol di- *p*-coumarate ester; d) maize lignin; e) a *threo-* β -ether-α -*p*-cournarate model; f) an *erythro-* β -ether- α -*p*-coumarate model. Spectrum g) is a stacked 3D plot of the same region as Figure d, showing the enormous acylated γ-position peaks but no detectable α-acylation in the highlighted region. HMQC experiments (Figures 13a-g) therefore established that lignin γ-units were acylated and that α-acylation was undetectable. HMBC experiments confimed that it was *p*-

coumarate that was acylating the lignin γ-positions. Figure 13h) to n) (see p. 96) are HMBC spectra showing correlation of the *p*-coumarate C9 carbonyl carbon with protons within three bonds, H-7 and H-8 of the *p*-coumarate moiety as well as those at the γ-position of the lignin sidechain: h) same model as a); i) same model as b); j) same model as c); k) maize lignin in which the *p*-coumarate carbonyl carbon clearly con-elates across the ester oxygen to the lignin γ-protons, unambiguously establishing the attachment of *p*-coumarate at the γ-position; 1) synthetic DHP showing a large amount of endgroups (A here), and identifying the comparable peak in the maize lignin; m) same model as e); n) same model as f). Figure 13o (seep. 96) illustrates *p*-coumarates strictly at the γ-positions of lignin sidechains, as elucidated by these NMR experiments. Color/structure assignments do not relate to those in other figures. Subsequent experiments with other grasses, derived from either C_3 and C_4 biosynthetic pathways, and including bamboo, reveal the same information — that acylation is entirely at the γ-position. The same finding has been recently published for wheat *(71)*. The only caveat with these observations is that the NMR experiments are performed on isolated lignins and not the entire lignin fractions. The small possibility exists that lignins acylated at the α-position were simply not extracted in the preparation. In the particular case of the maize lignin used for Figure 13, 67% of the lignin was extracted and utilized for NMR *(32)*. Solubilization in DMSO of the remaining material (not dioxane: water soluble) and crude NMR spectra indicated that the same features were present in the residue.

Cell wall cross-linking in grasses by ferulates

All grasses contain ferulate that is intimately incorporated into the cell wall, as has been recently reviewed *(72)*. Ferulates, acylating polysaccharides (primarily arabinoxylans), dimerize to effect polysaccharide-polysaccharide cross-linking *(72, 73)*. Both ferulates and ferulate dimers "attach" to lignins effecting polysaccharide-lignin cross-linking *(31, 37, 72, 74)*. A fraction of the ferulate can be released by high-temperature base, implying its incorporation as ethers *(60, 75, 76)*. Whether these ethers were α-ethers (and therefore products of simple nucleophilic addition of ferulates to intermediate quinone methides produced during lignification) or β-ethers (implying that they were intimately incorporated with normal lignin precursors via free-radical coupling processes) needed clarification. More detailed arguments can be found in several references *(21, 32, 37, 72, 77)*. NMR easily revealed that ferulates do intimately incorporate into lignins via radical processes *(37, 39, 72)*, as summarized below.

Synthetic lignin studies. Synthetic lignin (DHP) studies are enormously valuable in determining what types of reactions are possible and what types of products are produced. Data gained from DHP and model compound work are invaluable for

investigations into real plant materials. A model for ferulate on arabinoxylans was synthesized with strategic ^{13}C-labeling *(37, 78).* The[9–^{13}C] label allows NMR experiments to reveal what kinds of 8-coupling reactions are possible, but gives no data on coupling at the aromatic ring, 4-O- (aryl ethers) vs 5-/4-O- (phenylcoumarans). When a synthetic lignin from coniferyl alcohol was made in the presence of -5% of this labeled ferulate model, the single carbonyl resonance in the model produced some 5 environments in the DHP *(37),* Figure 14 (see p. 97). Figure 14 shows relevant portions of the inverse-detected long-range ^{13}C-^{1}H correlation (HMBC) spectra of the synthetic lignin along with model compounds for the various possibilities *(37).* The 1D carbon spectrum along the y-axis of the lower DHP figure is from a quantitative 1D experiment. Peak groupings are assigned to the structures from the models in the upper figures. The color coding does not relate to the standard assignments of Figure 2g each peak type was colored differently to distinguish them and to relate the peaks in the model spectra to the corresponding peaks in the DHP. Obviously, the ferulate was incorporating into more than just a single product. Long-range C-H correlation easily identified coupling modes. In particular, there are products in which the 8-position of fendate (analogous to the β-position of monolignols) was involved in radical coupling reactions to produce 8-5-, 8-O-4-, and 8-β-structures. All the expected products of radical coupling reactions can be observed *(37),* Figure 14 (see p. 97). The significance is that, since ferulate is incorporated into real plant lignins by radical coupling reactions, only a fraction of the ferulate (the 4-O-etherified components) will be releasable by solvolytic processes.

Ferulates in grasses. With the database of cross-coupling products from the above synthetic lignin studies, it becomes possible to look for these components in real lignins. Unfortunately, the levels are so low (a few percent of the lignin) and the *number* of products so diverse that spectra cannot easily show these products. However, NMR has sufficient dispersion and resolution to find the products if the signal to noise can be raised. Therefore, plants were grown in ^{13}C-enriched (~15%) CO_2 to provide uniformly labeled material *(39).* Such labeling is superior to any kind of specific labeling that might be envisioned since the plants' growth and metabolism are normal. Enrichment of ^{13}C in a sample to 15% provides a 15-fold sensitivity gain in ^{13}C NMR (and any 2D method that involves carbon), or a savings of $15^2 = 225$ in time to the same signal-to-noise. With such enhancements, the incorporated ferulates are readily discerned.

Figure 15a (seep. 98) is from an experiment run with an 80 ms long-range coupling delay. Processing was with Gaussian anodization (LB = -40, GB = 0.35) in t2 as a compromise for all correlations. Regions are labeled corresponding to regions in the synthetic lignin-FA-Ara polymer, Figure 14 (see p. 97). Overlaid are the data for

similar correlations in the FA-Ara DHP. Figure 15b) shows the 8-β-selection of a similar experiment run using a 110 ms long-range coupling delay which reveals the β- and 8-proton correlations more completely. Gaussian anodization in t2 used LB = -40, GB = 0.4. Numbering convention: numbering relates to that in the original ferulate (7-9 in the sidechain) and the original hydroxycinnarnyl alcohol (α, β, γ in the sidechain). When describing a dimer by its linkage, e.g. 4-O-β, the first term refers to the ferulate moiety and the second term to the lignin moiety. Figure 15b (see p. 98) shows the clear identification of the 8-β cross-product in ryegrass lignin. Interestingly, the 4-O-β -cross-coupled dimer was identified in the base-soluble fraction from grass straws *(79),* providing confirmatory evidence for the radical coupling mode. These products provide compelling evidence that ferulates are cross-coupling with normal monolignols during lignification in grasses.

A more intriguing observation than the presence of cross-coupling structures such as the 8-β -struchue, is the absence of other radical coupling products, notably the 8-5 and 8-O-4 Figure 15a *(39).* [Absence of peaks in correlation NMR experiments is not in itself diagnostic — peaks can be missing due to their coupling constants or other interactions, but the experiments here can be easily optimized for a certain product using the DHP sample. We are therefore cofident that the 8-5-coupled product is not present in the ryegrass lignin in any significant quantities.] What is important to note from Figure 15a is that resonances appear at the correct chemical shifts for all of the coupling products observed in the DHP. Without the benefit of these more diagnostic 2D experiments, it might have been concluded that all cross-coupling products were present in the ryegrass lignin. The importance of the observation that ferulate is found coupled at 4-O-, 5-/4-G-, and 8-β-, but not 8-5- nor 8-O-4 is that it strongly suggests that the ferulate in the wall is reacting only with monolignols and not preformed oligomers. This argument, and the suggestion that ferulates therefore act as nucleation sites for lignification in grasses, appears in more detail in published references *(39, 72).*

To illustrate further the power of NMR to provide detailed structural information, Figure 15c (seep. 98) shows how the same HMBC experiment reveals that ferulates cross-couple with both coniferyl and sinapyl alcohol monolignols *(39).* The identification of the 7- and α-protons of the cross-coupled dimer from their correlations with the carbonyl carbon (in Figure 15b), allows us to track their correlations in other areas of the spectrum. Thus, proton F7 would be expected to correlate with carbons F1, F2, and F6 on the ferulate ring, as it does, Figure 15c. More interestingly, H-α should correlate with carbons G1, G2, and G6 of a guaiacyl ring or S1 and S2/6 of a syringyl ring. In particular the S2/6 resonances are at much higher field (~105 ppm) than the G2 (~112 ppm) and G6 (~120) resonances, so that separation of correlations as belonging to syringyl or guaiacyl units is trivial. The

evidence that both monolignols reacted with ferulate was unexpected since ferulates were suggested to be involved in early wall development whereas syringyl units resulted later *(59, 80, 81).*

Lignins from (Z)-coniferyl alcohol

As has been noted previously *(82),* like the normal *(E)*-coniferyl alcohol, *(Z)*-coniferyl alcohol can polymerize via single-electron oxidation to produce a lignin-like polymer, but the obvious structural questions were not addressed; in particular, does the sidechain in end-group units retain the *(Z)*-geometry, and are units such as phenylcoumarans and resinols formed with the same ring stereochemistry? After developing a new synthesis for *(Z)*-coniferyl alcohol, we prepared a synthetic lignin (DHP) and examined it by NMR.

Figure 16 (see p. 99) shows the sidechain region of 2D HMQC-TOCSY spectra of acetylated synthetic lignins prepared from *(E)-* and *(Z)*-coniferyl alcohols. As described above, such spectra correlate a carbon with its attached proton and all protons within the same coupling network as that attached proton. They consequently give redundant information which is particularly valuable for tracing out lignin substructures. Lignin units A-E (shown in their unacetylated forms) are identified, along with coniferyl alcohol endgroups X, the *(E)*-cinnamyl alcohol sidechain, and X', this *(Z)*-sidechain. Contours at cabon frequencies labeled U1 and U2 are currently unassigned. The small amount of dihydroconiferyl alcohol endgroups Y in the *(E* -coniferyl alcohol lignin are from a 2% dihydroconiferyl alcohol impurity in the monomer. The *(E)*-cinnamyl alcohol endgroups X (~5% of the X' contours) in the are presumed to arise from the 2% *(E)*-coniferyl alcohol that was in that monomer. Color/structure assignments are as in Figure 2g.

As seen in Figure 16b (see p. 99), all of the interunitary linkages are represented in the *(Z)*-coniferyl alcohol polymer and appear to be the same isomers that are traditionally observed in synthetic and natural lignins from *(E)*-coniferyl alcohol, although they are present in different proportions. The striking difference comes from the remaining unsaturated sidechains X or X' which arise from coupling of monomers at other than their β-positions. These sidechains retain the geometry of the parent coniferyl alcohol. However, such units are minor in real lignins where monomers seldom encounter other monomers. No lignin examined to date reveals authenticated detectable *(Z)*-sidechains. Unknown structures also appear to have been produced from *(Z)*-coniferyl alcohol that have similarities to β-ether and β-5 products but unusual carbon shifts. Further work will be required to elucidate their structures and to determine if such structures are found in plant lignins.

**Products in lignins from mutant or genetically altered plants**

Various plants with deficiencies in lignin-biosynthetic-pathway genes (and consequent enzymes for monolignol synthesis) have recently become of interest *(83)*. Figure 17. They provide insights into the flexibility of the lignification process and aid in our understanding of "normal lignification. There is currently some discussion over whether lignins isolated from these plants are true structural lignins *(84),* but here we will use these "lignins" as examples of the value of NMR to elucidate the novel structures contributing to these intriguing polymers.

Figure 17: Lignin biosynthetic pathway, simplified schematic. Not all of the pathways or enzymes are necessarily known or distinct. CAD (cinnamyl alcohol dehydrogenase) is a generic term for the enzyme class that catalyses the final reduction to hydroxycinnamyl alcohols—CAD' may or may not be different from CAD and CAD". Similarly for CCR (cinnamoyl-CoA reductase) and other enzymes.
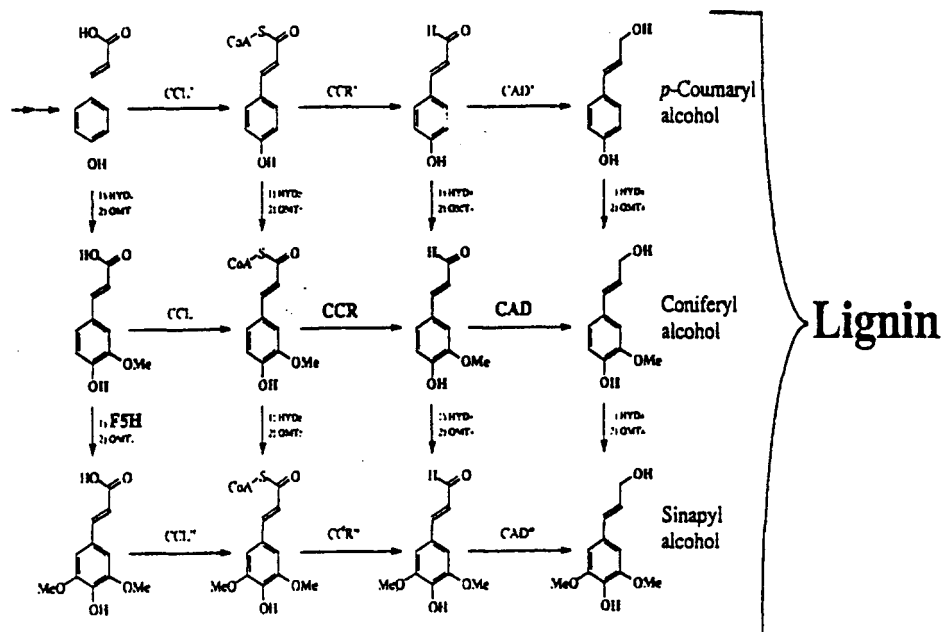
S:G Changes in Arabidopsis F5H Mutant and Transgenic. Chappel's group have described an Arabidopsis mutant deficient in ferulate 5-hydroxylase (enzyme F5H, gene *f5h) (85),* the first enzyme that controls the production of sinapyl alcohol and therefore syringyl units. This mutant, derived from chemical mutagenesis, has virtually no syringyl component in its lignin. When a suitably promoted *f5h* gene was introduced into the normally F5H-deficient mutant, up-regulation of sinapyl alcohol production was at such a high level that the lignin became extremely syringyl-rich, and contained only a minor guaiacyl component..

Figure 18: HMBC spectra of lignins from Arabidopsis, showing how syringyl:guaiacyl ratios can be manipulated using the ferulate 5-hydroxylase gene *(85).* **Correlations for the β-either unit A α-proton are shown. The wild type control has a guaiacyl-rich lignin. The** *f5h* **mutant has extremely low levels of S units, detectable only at lower contour levels. The** *f5h⁺* **transgenic has the** *f5h* **gene re-introduced in to the** *f5h* **mutant; syringly levels return close to wild-type. Using a different promoter, the** *f5h⁺⁺* **transgenic has up-regulated syringyl lignin production almost to the exclusion of guaiacyl lignin.**
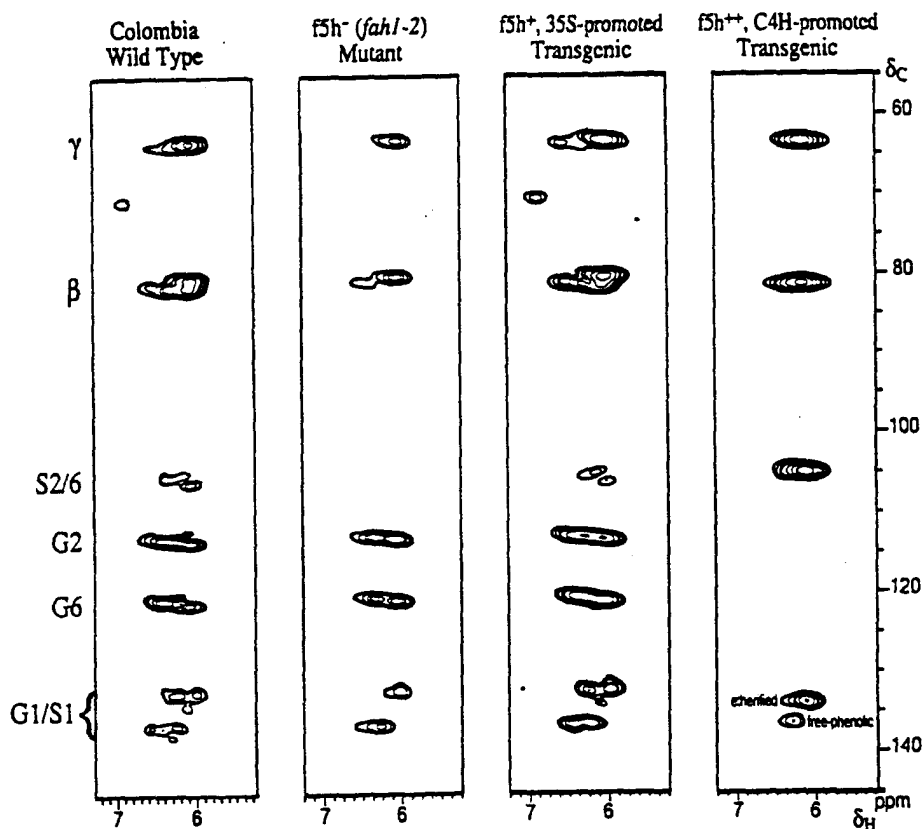
Comparing 1D spectra is of come revealing, but to illustrate the value of information provided by 2D experiments, we show here the S:G insight gained from looking at correlations in a long-range ^{13}C-^{1}H correlation (gradient-enhanced HMBC) experiment. Figure 18 shows the correlations between the α-protons of the major β-aryl ether units in lignins from each of four samples; wild-type control, down-regulated mutant *(f5h)*, a 35S-promoted up-regulated *f5h* transgenic *(f5h$^+$)* and a C4H-promoted up-regulated *f5h* transgenic *(f5h^{++})*. As expected, the α-protons correlate with carbons β and γ of the sidechain and carbons 1, 2 and 6 of the aromatic rings; all of these carbons are within 3-bonds of the α-proton. What makes these correlation spectra useful is that the equivalent syringyl S2/S6 carbons, resonating at ~105 ppm, are well separated from their guaiacyl counterparts (for which G2 and G6 are different, at ~110 and ~120 ppm). Thus it is immediately clear that the control contains guaiacyl and syringyl (β-ether) units. The *f5h* mutant has almost no syringyl component. The *f5h^{++}* lignin is extraordinary. The lignin is extremely syringyl-rich; only weak guaiacyl peaks can be discerned at lower levels. The up-regulation is therefore strikingly effective at diverting the monolignol pool into almost entirely sinapyl alcohol. In fact the syringyl:guaiacyl ratio in this transgenic is higher than has been recorded in any plant to date.

CAD-deficient Tobacco. Boudet *et al.* have downregulated CAD (cinnamyl alcohol dehydrogenase, see Figure 17) by antisense technologies *(86)*. The major difference between extracted lignins from normal vs antisense-CAD tobacco is in aldehyde components *(38)*. The benzaldehyde U and cinnamaldehyde V peaks normally present are elevated and new aldehydes W become major components, Figure 19b (see p. 100). Aldehydes W appear to be dimers of cinmmaldehydes. Peak Wb, Figure 19b, matches data from a synthetic 8-O-4-dimer of coniferaldehyde, and peak V also belongs with this dimeric unit peak Wa is suspected to be the 8-O-4cross-coupled product with a normal G- or S-unit. The interest in this case is whether the aldehyde peaks are from coniferaldehyde or sinapaldehyde. As in the case of ferulate cross products described above, this can be determined from long-range correlation (HMBC) spectra. As seen in Figure 19c, the new aldehydes in the antisense-CAD tobacco appear to be mostly syringyl products implying that the targeted CAD enzyme is responsible for reducing sinapaldehyde as well as coniferaldehyde.

Figure 19c (see p. 100) also illustrates how the previously unknown components W were erroneously attributed to 2-methoxybenzaldehydes *(23)*. Firstly, the aldehyde carbon chemical shift was very low, ~188 ppm. A literature search for aldehyde carbons at this position only unearthed 2-methoxybenzaldehdes at those positions. HSQC-TOCSY spectra indicated that only a single proton was within 3-bonds; the structure therefore seemed like a benzaldehyde. To essentially 'confirm' the

assignment, the HMBC experiment Figure 19c, showed that carbons (now labeled C-8, but originally thought to be C-2 of the 2-methoxybenzaldehyde) were each within three bonds of both the aldehyde proton and by fairly convincing correlations, methoxy protons. Only a 2-methoxybenzaldehyde seemed to fit all these requirements leading us to make the tentative assignment despite the troublesome biochemical implications. In subsequent studies, we found that the methoxy correlations were merely accidentally coincident and that the aldehydes belong to coniferaldehyde or sinapaldehyde 8-O-4-products W *(38),* much more logical products given the increased amount of aldehydes that accumulate when CAD is deficient.

CAD-deficient Pine. MacKay *et al.* have identified a pine that is naturally deficient in CAD *(87).* This lignin has elevated aldehyde levels, as does the antisense-CAD tobacco lignin described above, and has analogous cimamaldehyde dimers, from coniferaldehyde in this case *(23).* But more interesting is the enormous elevation of an unexpected component, dihydroconiferyl alcohol (DHCA) *(23).*

Figure 20 (p.101) shows a picture of wood chips from normal pine and a homozygous mutant with reduced CAD activity exhibiting the brown wood phenotype. To the right are stem sections of 2-year old trees immediately after debarking. The cad-n1 mutant is readily identified by the red-brown color of its wood. Figures a) to c) show regions of HMQC-TOCSY spectra of unacetylated milled wood lignins from a) the pine cad-nl mutant, b) from a cad-normal wood, and c) from a synthetic lignin. Structure assignments are most easily seen in spectrum 20c from the synthetic lignin which derived from coniferyl alcohol containing ~2% dihydroconiferyl alcohol. Although synthetic lignins of this type have quite different substructure ratios from plant lignins, they contain all of the structural units and are valuable for spectral assignment. Thus in Figure 20c, β-aryl ether units A, α,β-aryl ethers E (scarce in plant lignins), phenylcoumarans B, and resinols C are readily identified, along with coniferyl alcohol endgroups X, and the dihydroconiferyl alcohol units Y. In the CAD mutant, dihydroconiferyl units Y are dominant, displacing much of the intensity from the normal coniferyl alcohol-derived region. Some of the minor units can be seen in the pine samples when looking at lower contour levels (not shown). The normally predominant β-aryl ether A and phenylcouxnaran B components, Figure 20b, are severely reduced in the cad-n1 mutant, with only some β-ether peaks being observable at comparable contour levels — these may also arise from *p*-coumaryl alcohol (in addition to coniferyl alcohol). Grey contours are from intense methoxyl signals, carbohydrate impurities, and other lignin structures not discussed here. Figure 20d shows aldehyde carbonyl group congelations from the HMQC-TOCSY spectrum of lignin from the cad-n1 mutant plant showing the presence of cinnamaldehyde V (with correlations to the three sidechain protons) and benzaldehyde U (single correlations) units in the lignin. The normal pine lignin carbon section is shown to the

left. The ^{13}C-spectra shown on projections to the left of the figure are normalized to the same methoxyl level; cinnamaldehyde V and benzaldehyde U signals are approximately twice as abundant in the mutant. The higher field aldehydes W dramatically increased in the mutant are identified as 8-O-coupled coniferaldehyde units, consistent with the buildup of coniferaldehyde in this mutant. Color/strucrure assignments are as in Figure 2g, except that Y' uses the color usually reserved for units F.

In addition to the obvious paucity of normal lignin units in the mutant's lignin, the striking difference is the dihydrocimamyl units Y. Furthermore, these units are present in two distinct environments, only one of which is represented in the normal pine, as shown in Figure 21 (see p. 102). Correlations Y match those of DHCA-coniferyl alcohol β-5 and β-O-4 crossed products (but don't forget that *p*-coumaryl alcohol is a significant component too). Correlations Y' match correlations in homo-coupled DHCA. In the normal pine where the levels of DHCA are low, these Y' correlations cannot be detected. They are present in the DHP which has about 2% DHCA, and where dimerization is common. The huge elevation in the DHCA level in the CAD-deficient mutant presumably provides for significantly more homo-coupling to produce an abundance of structures Y'. Colors in Figure 21 do not relate to those in other figures.

About 50% of the DHCA units are in 5-5-coupled structures, Figure 21 (see p. 102). This fact, along with the observation of the dihydroconiferyl alcohol monomer in solvent extracts, strongly indicates that DHCA is a monomer in the mutant pine lignification and not some product of post-coniferyl alcohol-coupling reactions, as has been suggested *(88)*. Strongly worded comments claiming DHCA is not a component of the polymer and that the lignins were merely dioxane:water-extractable oligomerized lignan artifacts can also be refuted by NMR work. It was claimed that the DHCA we found in the isolated lignin represented less than 5% of the total lignin *(88)*. This "recalculation" noted that we extracted ~17% of the lignin in soluble form suitable for NMR, and that we claimed that the isolated lignin was ~30% DHCA-derived. The recalculation however assumes, quite incorrectly, that the DHCA was completely extracted (as an "artifact") and that the remaining lignin is devoid of this component. In a cyclic argument, the *assumption* that it is an artifact is used to prove that it is an artifact !

We presented other analytical data to support the presence of DHCA throughout the lignin fractions *(23, 89)*. The insolubility of the lignins remaining following dioxane:water extraction presents a significant challenge, but some success has been possible using various solubilizing techniques. For example, we were able to dissolve the residual lignin from the CAD-deficient mutant pine in acetyl or propionyl

bromide *(90)*. These reagents acylate and α-brominate the lignin, and cause some other structural changes, but in no way (other than acetylation) affect the saturated aryl propanol side-chain. Various NMR experiments then unambiguously determined that DHCA was a component of that lignin. For example, Figure 22 (see p. 102) shows a TOCSY spectrum, illustrating clearly the full coupling network of the DHCA sidechain Y. With carbon chemical shifts also verified via HSQC spectra (not shown), the presence of DHCA units Yin the residue is well authenticated allaying criticisms that it may be only an extractable artifact. Further work is aimed at quantifying the DHCA component in both lignin fractions, and determining if it is associated with high-molecular-mass lignin.

CCR-deficient Tobacco. CCR (cinnamoyl-CoA reductase, see Figure 17, p. 78) has also been downregulated in tobacco by antisense methods *(91)*. That lignin, present in the plant and extractable in much lower amounts (~50%), also shows a striking increase in a non-traditional component. NMR, with valuable insight from thioacidolysis observations, reveals the enhanced component to be derived from tyramine cinnamates, primarily tyramine ferulate.

Figure 23 (seep. 103) shows various spectra of nomal and CCR-deficient, as well as CAD-deficient, tobacco lignins. ^{13}C NMR spectra of a) normal and b) antisense-CCR tobacco isolated lignins (unacetylated) reveals the extent of the elevation of the tyramine ferulate component in the transgenic, Figure 23b. Figures c) to e) are partial 2D HSQC (gradient selected) spectra Interunit types A-E are apparent in all spectra. Endgroups are not all visible in the sidechain region shown. These isolated tobacco lignins resemble synthetic lignins more than any lignin charaterized by NMR to date; they have significant numbers of α,β-diether E units, and unsaturated sidechains X, indicating frequent dimerization reactions of monolignols. Other plant isolated lignins have low levels of these units and arise from endwise coupling of hydroxycinnamyl alcohol units with growing lignin oligomers. Evidence for coniferyl alcohol depletion is seen in both antisense lignins.

Whereas aldehydes (not visible in this range) are the major feature of the antisense-CAD lignin, tyramine units Z are strikingly enriched in the antisense-CCR lignin. The proof for tyramine ferulates is in the spectra of Figure 23g-h. Figure 23g) shows a partial 2D HMQC-TOCSY NMR spectrum of the antisense-CCR tobacco isolated lignin (acetylated) proving tyramine units are involved as amides. Correlation between the tyramine sidechain aliphatic carbons (Cα and Cβ) and the three sidechain protons (Hα Hβ, and the amide N-H) matches well with data from tyramine ferulate itself (superimposed data in green). Figure 23h provides proof that feruloyl units are amides with tyramine. HMBC spectra show diagnostic correlations between the amide carbonyl to ferulate H7 and H8 sidechain protons (as well as the

83

Ralph, Marita, *et al.*

amide NH, close to H8) and, across the amide bond to the Hβ protons on tyramine, proving that the tyramine and ferulate are linked. Determination of the full array of feruloyl unit linkages awaits preparation of synthetic lignins containing strategically labeled tyramine ferulate. Colors in figures g and h do not relate to structure assignments in Figure 2g.

Whether the tyramine ferulate is truly incorporated into structural lignin, into suberized components *(92),* or simply represents polymerized secondary metabolites similar to those observed in a wounding response are important issues not addressed here. However, the aliphatic components normally associated with suberins are not significant in these extracted Lignins. Also, tyramine components are not elevated in the antisense-CAD tobacco (Figure 23d, see p. 103; Figure 19b, see p. 100) which was presumably similarly stressed.

Identification of new structures in lignins

Of all the units identiled, the identification of dibenzodioxocins D in lignins has been the most exciting recent development *(33, 34).* It provides a new pathway for 5-5-linked units to be incorporated into cyclic ether structures. Despite being ethers, such structures cannot necessarily be fully released by solvolytic methods. NMR was crucial to the identification of the novel units and to the unambiguous demonstration of their presence, at significant levels, in (isolated) lignins. A survey of plants reveals that dibenzodioxocins are present in all lignin classes (from softwoods and hardwoods as well as grasses and legumes, as seen here) *(93).* Representative spectra from the major classes, with the dibenzodioxocins highlighted in red, are shown in Figure 24 (seep. 104). Our group was originally concerned that such units could be artifacts of acetylation since they were difficult to find in unacetylated samples, yet readily showed up in acetylated samples. The reason appears to be that the chemical shifts are more variable in unacetylated samples, smearing out the required correlation peaks. They sharpen a little in DMSO (Ralph 1998, unpublished).

Dibenzodioxocins D show up easily in HMQC or HSQC spectra, where the Cα–Hα and Cβ-Hβ correlations are unique and readily identified. Figures 24b-g are HSQC spectra representing various classes of lignins: b) from the acetylated "methoxy-less" DHP described in Figure 3 (seep. 90); c) *Pinus taeda* acetylated milled wood lignin; d) from the CAD-deficient *Pinus taeda* mutant described in Figure 20 (seep. 101) - note the enhanced dibenzodioxocin levels due to the high levels of 5-5-linked DHCA units in this lignin; e) a non-acetylated (the reason for the different peaks of structure D!) synthetic DHP derived from coniferyl alcohol and 5% [9-^{13}C]5–5-diFA-Ara, a 5-5-coupled dimer of a ferulate-arabinofuranoside ester *(31);* f) a ryegrass acetylated lignin known to contain diferulates and therefore likely to contain dibenzodioxocins

84

derived from 5-5-coupled diferulate *(39);* g) an acetylated aspen lignin. Color/structure assignments are as in Figure 2g. Dibenzodioxocins D are also identified in the tobacco lignin spectra of Figure 23 (see p. 103). Due to diverse proton-proton coupling constants, the full sidechain correlation matrix does not always show up well in HSQC-TOCSY experiments with typical (80-100 ms) TOCSY mixing times, *e.g.* Figure 8a (see p. 93). Figure 24a shows an HSQC-TOCSY acquired using a 125 ms TOCSY mixing time, which beautifully emphasizes the full D coupling array.

Recently we made a tentative discovery of a similar, although less prominent, product with interesting implications for the β-1 coupling pathway *(94, 95)*. Aryl isochromans can be reasonably easily identified in some softwood isolated lignins by their diagnostic HMQC or HSQC correlation at δ_C 41.3, δ_H 3.60 (acetylated units, in acetone). The complete sidechain of the crucial unit is seen in TOCSY spectra. Figure 25 (see p. 86) shows the sidechain region of a TOCSY (spin lock time, 100 ms) spectrum of *Pinus taeda* acetylated milled wood lignin clearly delineating the Hα-Hβ-Hγ1-Hγ2 coupling network for new aryl isochroman structures derived from β-1-coupling. Correlations from an authenticated compound containing the isochroman structure *(94, 95),* isolated from DFRC degradation, are at the center of the overlying circles. Other correlations present but not fully resolved are shown with dotted circles.

The five pieces of concurrent NMR data (δ_{Cb}, δ_{Ha}, δ_{Hb}, δ_{Hg1}, δ_{Hg2}) validate the presence of aryl isochroman in the milled lignin isolate. The structure was first noted and identified in the trimeric fraction from degradation of pine wood using the DFRC (derivatization followed by reductive cleavage) method *(94, 95)*. Whether it is present as such in native lignins is not yet clear, but even if not the internal trapping of a β-1 quinone methide intermediate (Figure 24, bottom scheme) is presumably operating *in vivo*. The structure differs from structures previously assigned as β-6/α-1-isochromans — we have evidence that the regiochemistry assigned to those structures identified in hydrogenolysis and thioacidolysis products may be incorrect, *i.e.* that they are probably β-1/α-6 compounds *(94)*. The rational mechanism for formation of such aryl isochromans is given in Figure 25 (see p. 86), and more fully elsewhere *(94)*.

Figure 25: Sidechain region of a TOCSY (spin lock time, 100 ms) spectrum of *pinus taeda* acetylated milled wood lignin, clearly showing the H-α/H-β/H-γ1/H-γ2 coupling network for new aryl isochroman structures derived from β-1-coupling. Correlations from an authenticated compound containing the isochroman structure *(94, 95),* isolated from DFRC degradation, are at the center of the overlying circles. Other correlations present but not fully resolved are shown with dotted circles. Bottom: Abbreviated scheme for formation of aryl isochromans following β–1-coupling.
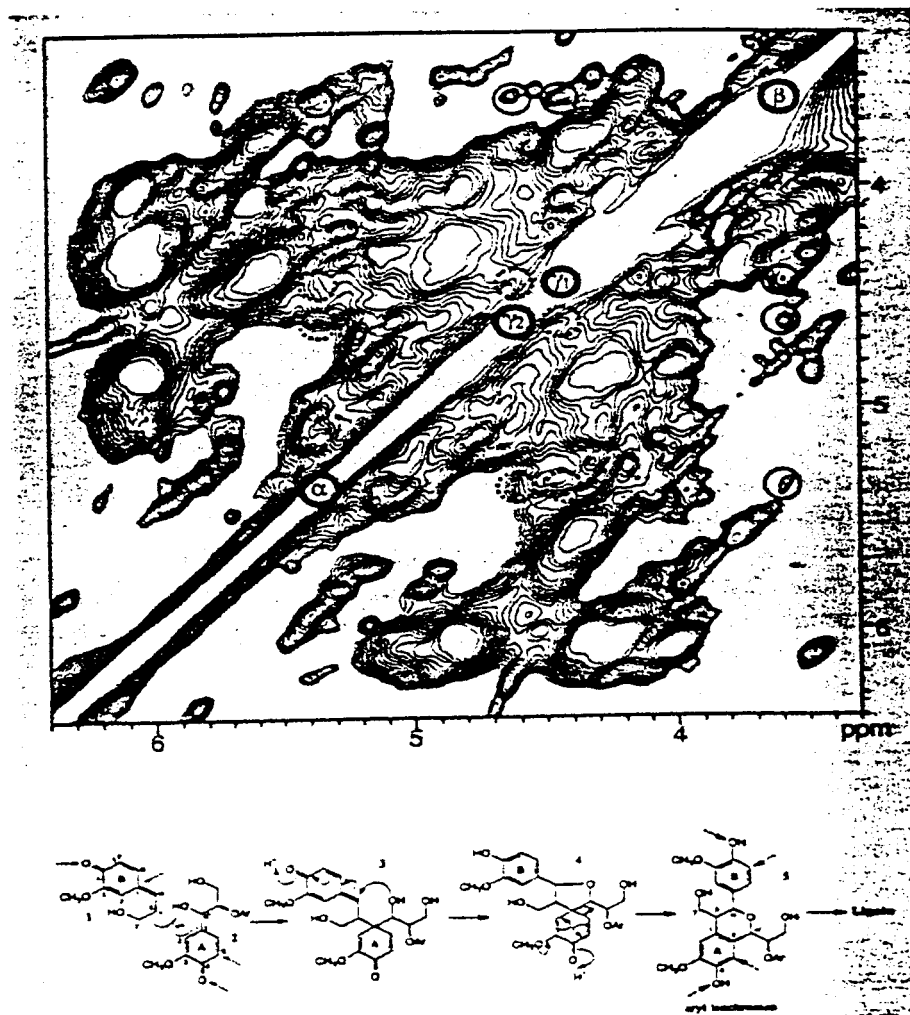
Conclusions

NMR has been an indispensable tool in lignin and cell wall research. Structural identifications, of the types illustrated here, are often key observations leading researchers to identify biochemical pathways. There is little question that NMR is one of the most diagnostic tools, providing often unambiguous evidence for structures that would require less elegant solutions by other methods. Of course, it cannot stand alone as the single tool for all structural questions. It has significant limitations. NMR is orders of magnitude less sensitive than other spectroscopic methods. However, with the variety of expedients available, the information content is much higher than from any other instrumental method, and its meager sensitivity is sufficient for many studies. Sample isolation and solubilization are required for solution-state NMR. Solid-state NMR has the potential to analyze intact samples and recent advances suggest that there will be important new applications. But the kind of structural detail revealed in the examples here is only available through high-resolution solution-state NMR studies. With the current availability of a huge number of pulse experiments, only a few of which were touched on here, and the commercial availability of powerful spectrometers with increasingly sophisticated features, there is little doubt that NMR will continue to play a pivotal role in plant lignin and cell wall structural studies.

Experimental

Most spectra shown here were generated in our laboratory at the US Dairy Forage Research Center, on a Bruker AMX-360 or, more recently, an (upgraded) Bruker DRX-360 (with a fully digital system and gradients); 750 MHz spectra were run on a Bruker DMX-750 at the University of Wisconsin-Madison National NMR facility. All experiments used stock Bruker pulse programs, with important parameters noted in the text or figure captions.

Ralph, Marita, *et al.*

Acknowledgement

Color Figures

Figure 2: Four-minute ID and 2d spectra. (seep. 56-57).

a) DHP, 4 min ^{13}C

d) Pine lignin, 4 min ^{13}C

b) DHP, 4 min HSQC

e) Pine ML, 4 min HSQC

c) DHP, 4 min HSQC (sidechain region)

f) Pine ML, 4 min HSQC (sidechain region)

g) Color assignments

Interunit Types

A β-aryl ether (β-O-4)
B phenylcoumaran (β-5)
C resinol (β-β)
D dibenzodioxocin (5-5/β-O-4,α-O-4)
E α,β-diaryl ether
F α-keto-β-aryl ether (β-O-4)

Not assigned or saccharides

Methoxyl

U benzaldehyde
V cinnamaldehyde

Endgroups

X (E)-cinnamyl alcohol
Y dihydrocinnamyl alcohol (aryl propanol)

89

Figure 3: Comparison of 2D NMR spectra of synthetic lignins from normal (left) and "methoxy-less" (right) coniferyl alcohol. (seep. 58).

90

Figure 5: TOCSY spectra of a) an acetylated coniferyl alcohol synthetic lignin (DHP) and b) an acetylated *Pinus taeda* lignin. (see p. 61)

Figure 6: Proton J-resolved spectra of a) an acetylated coniferyl alcohol DHP and b) an acetylated pine isolated lignin. (seep. 62).

Legend
— A: β-aryl ether (β-O-4)
— B: phenylcoumaran (β-5)
— C: resinol (β-β)
— D: dibenzodioxocin (5-5/β-O-4,α-O-4)
— E: α,β-diaryl ether
— X: (E)-cinnamyl alcohol endgroups
— Y: dihydrocinnamyl alcohol endgroups
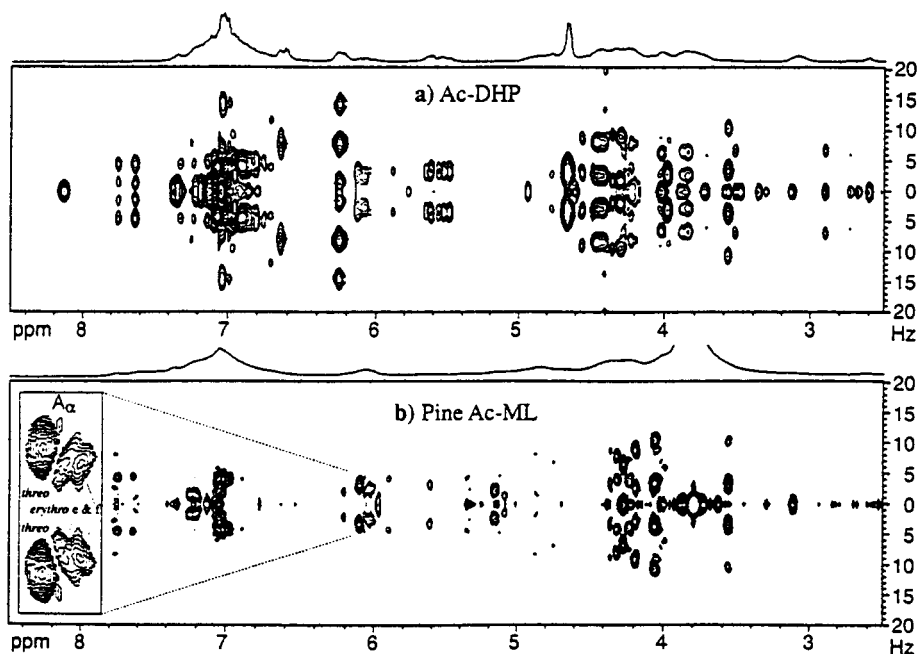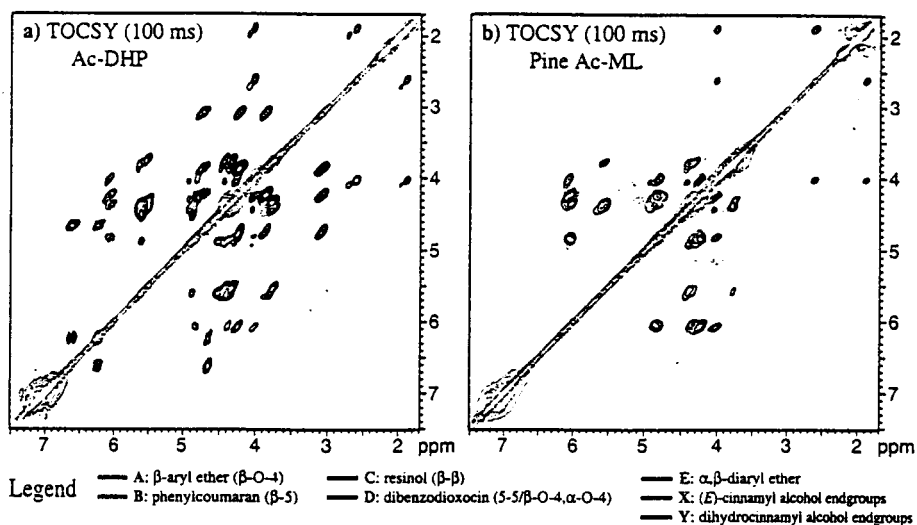
Figure 7: HSQC (gratient) spectra of various lignins showing major structural units A-E, X. (seep. 63).
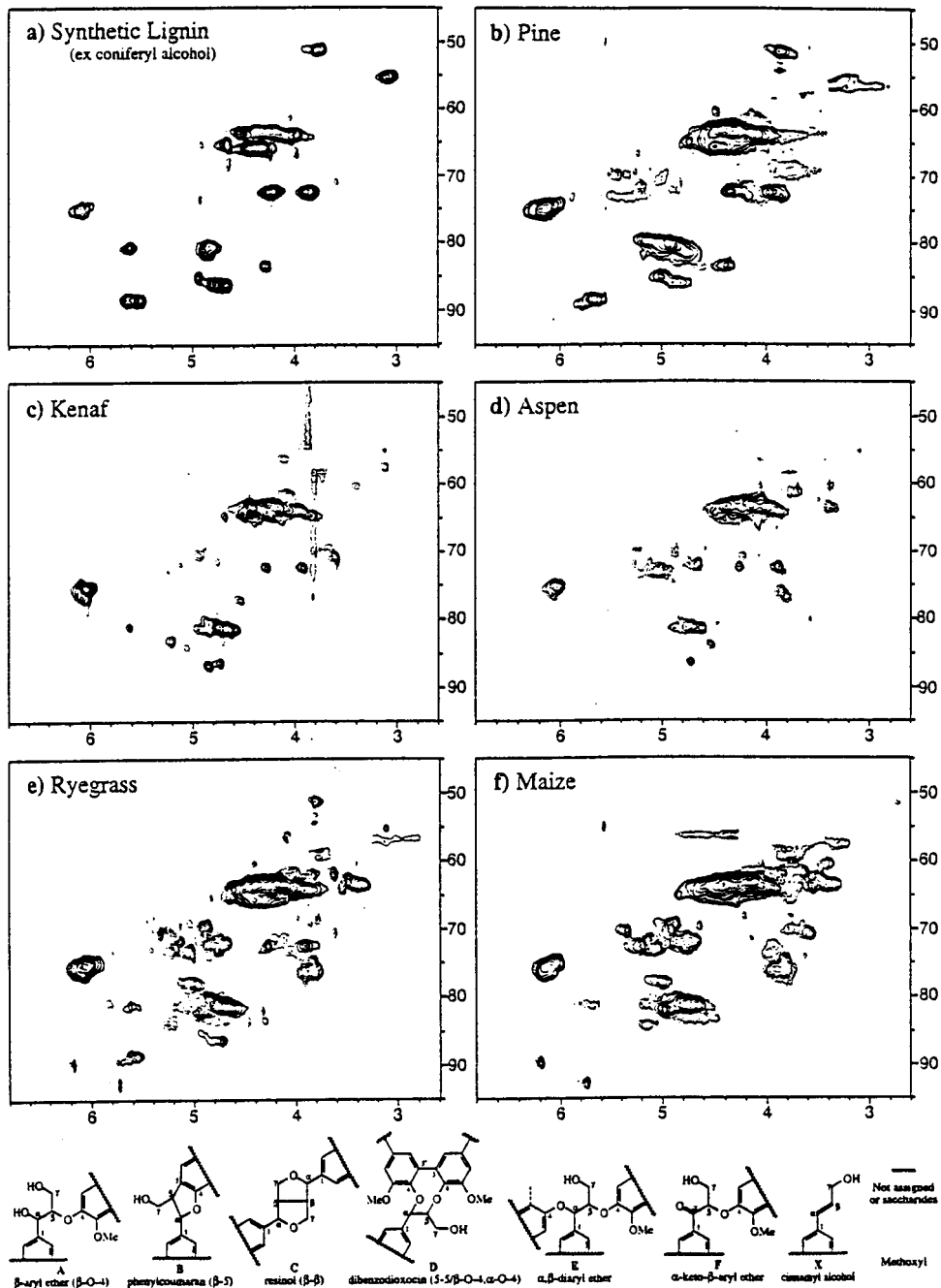
**Figure 8: HSQC-TOSCY (gradient) of lignins used in Figure 7. **

**Figure 9: HMBC spectrum, partially color-assigned, of the acetylated synthetic lignin sample of previous figures. **

Legend
— A: β-aryl ether (β-O-4)   — C: resinol (β-β)   — E: α,β-diaryl ether   — Y: dihydrocinnamyl alcohol
— B: phenylcoumaran (β-5)   — D: dibenzodioxocin   — F: α-keto-β-aryl ether   — X: (E)-cinnamyl alcohol

Legend   — A: β-aryl ether (β-O-4)   — B: phenylcoumaran (β-5)   — C: resinol (β-β)
          — E: α,β-diaryl ether   — X: (E)-cinnamyl alcohol
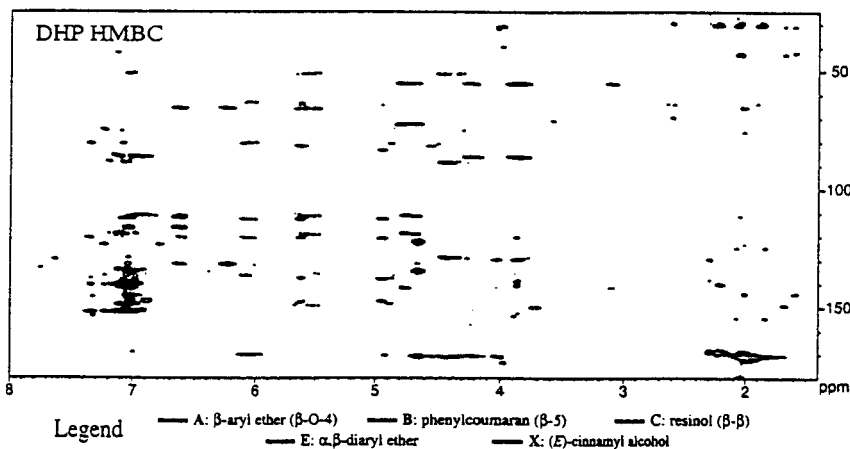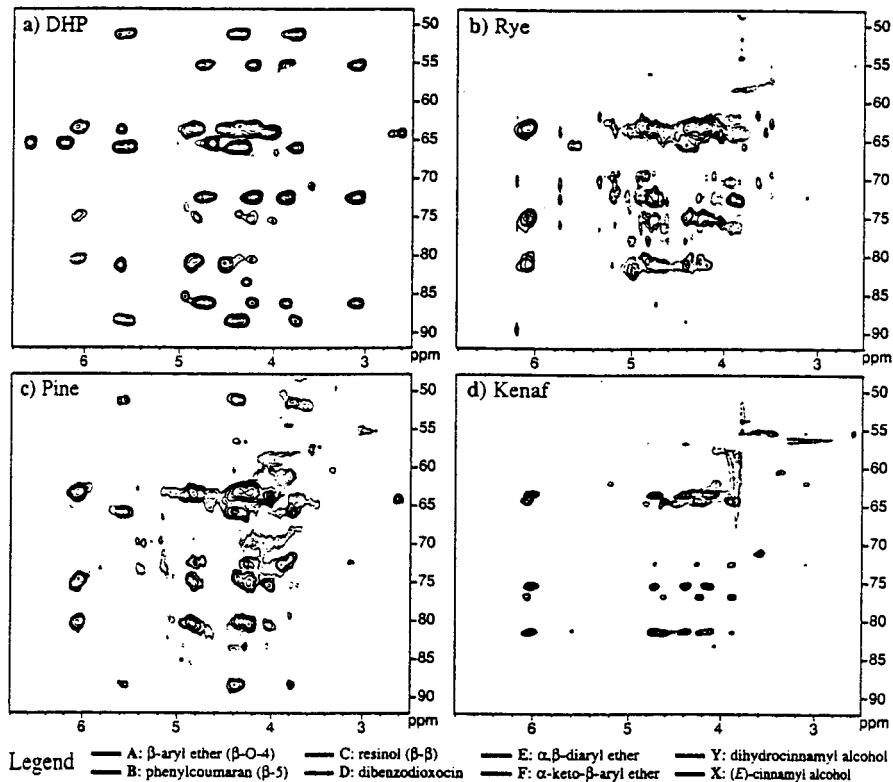
Figure 11: a-e: 3D-HMQC-TOCSY experiment (100 ms TOCSY) on a synthetic DHP, at natural abundance. (seep. 68).
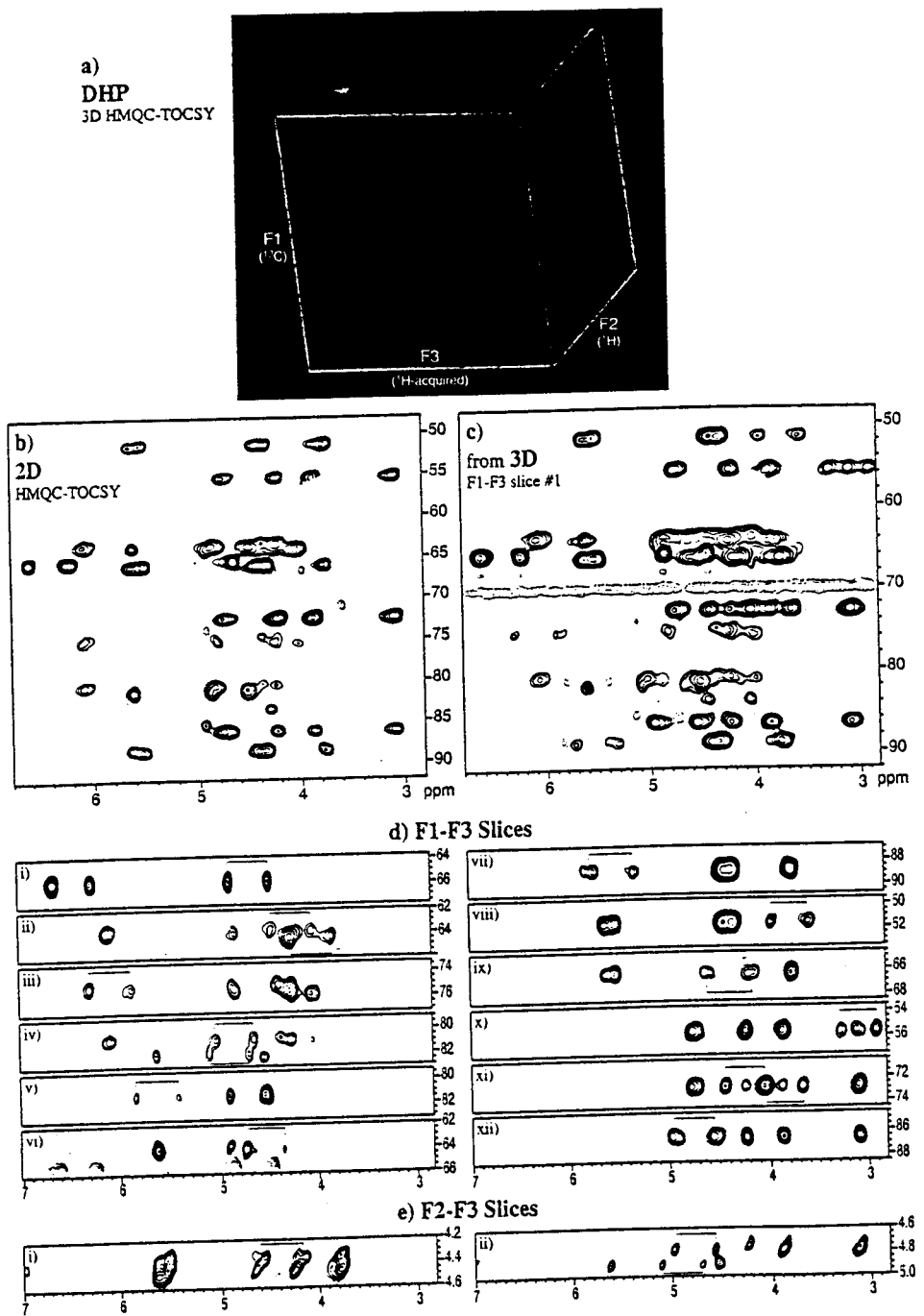
Figure 12: Spectra from *Tainung kenaf* bast fiber isolated lignin. (see p. 72).
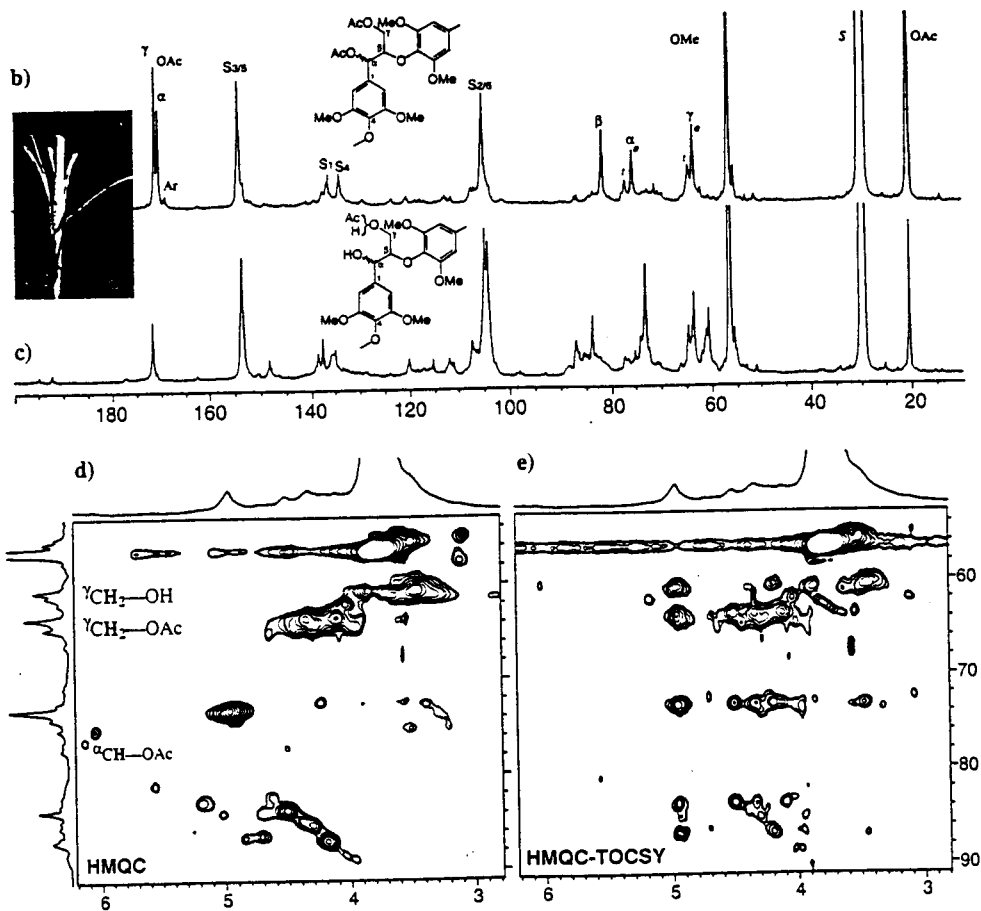
Figure 13: Spectra of models and maize lignin showing acylation by p-coumarate strictly at the position. (see p. 73).
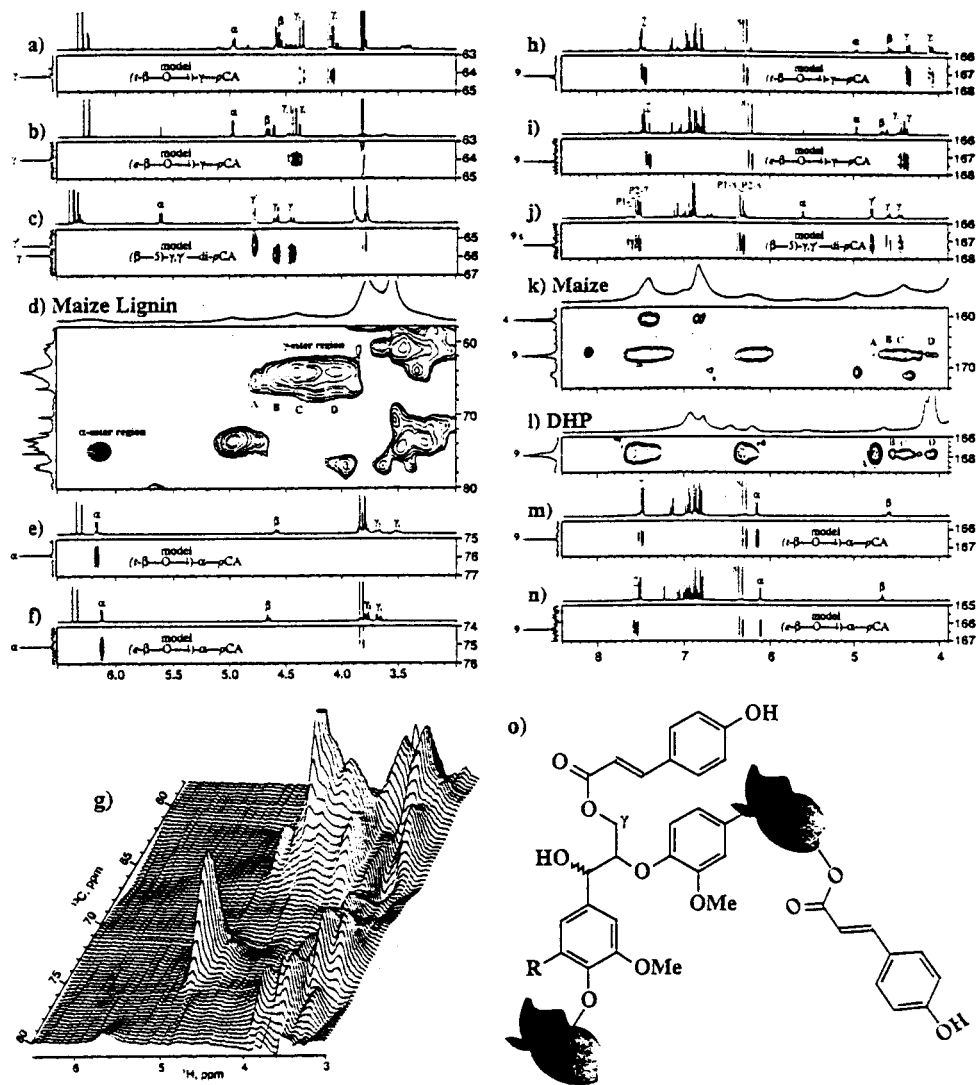
Figure 14: Partial HMBC spectra of a synthetic lignin prepared from coniferyl alcohol and 5% [9-^{13}C]ferulate-arabinofuranoside ester along with model compounds for the various radical coupling possibilities. (see p. 75).
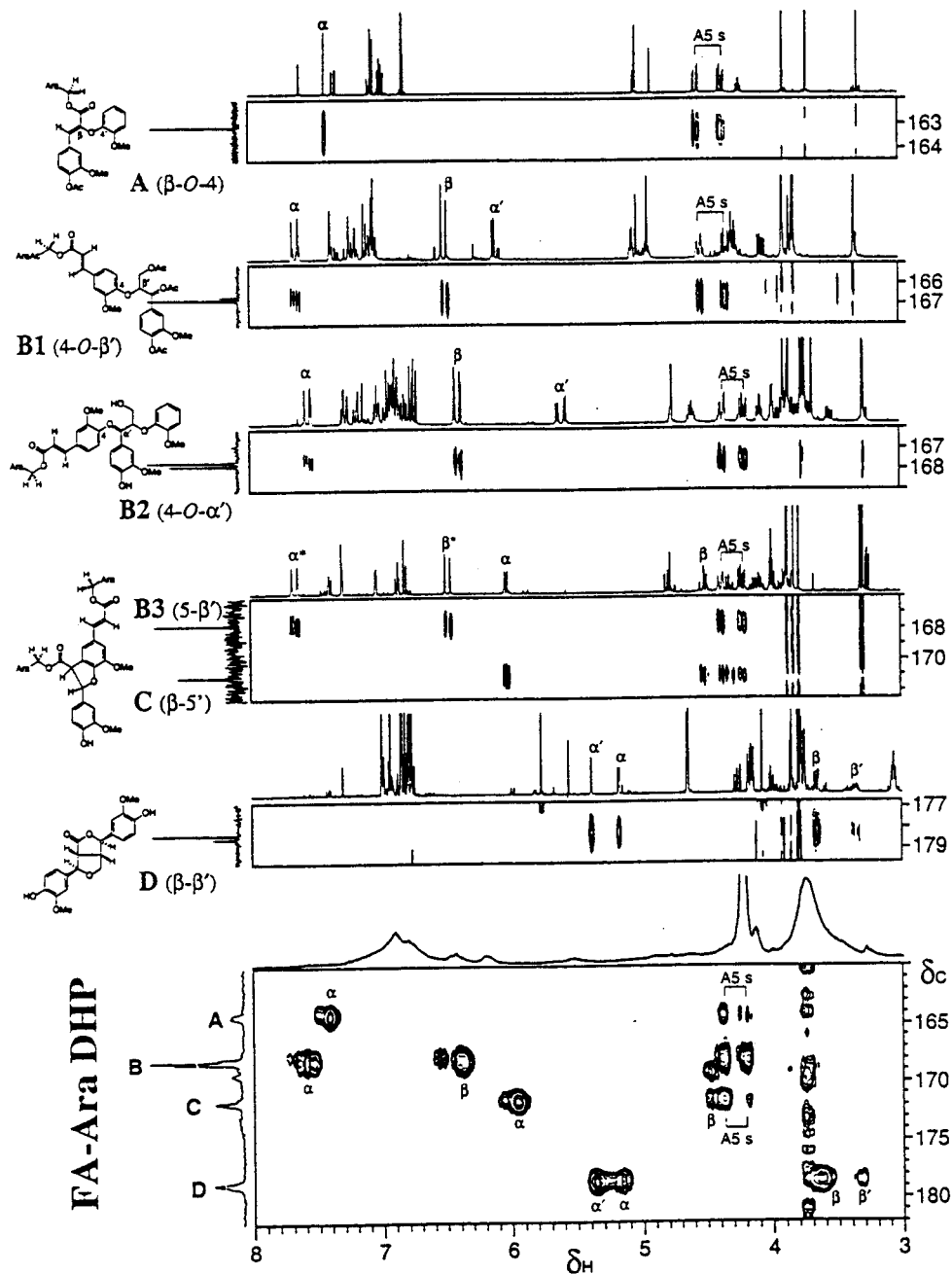
Figure 15: HMBC spectra of uniformly 13C-enriched ryegrass lignin providing evidence for radid coupling of ferulate into the lignin, and for its coupling with both coniferyl and sinapyl alcohols.
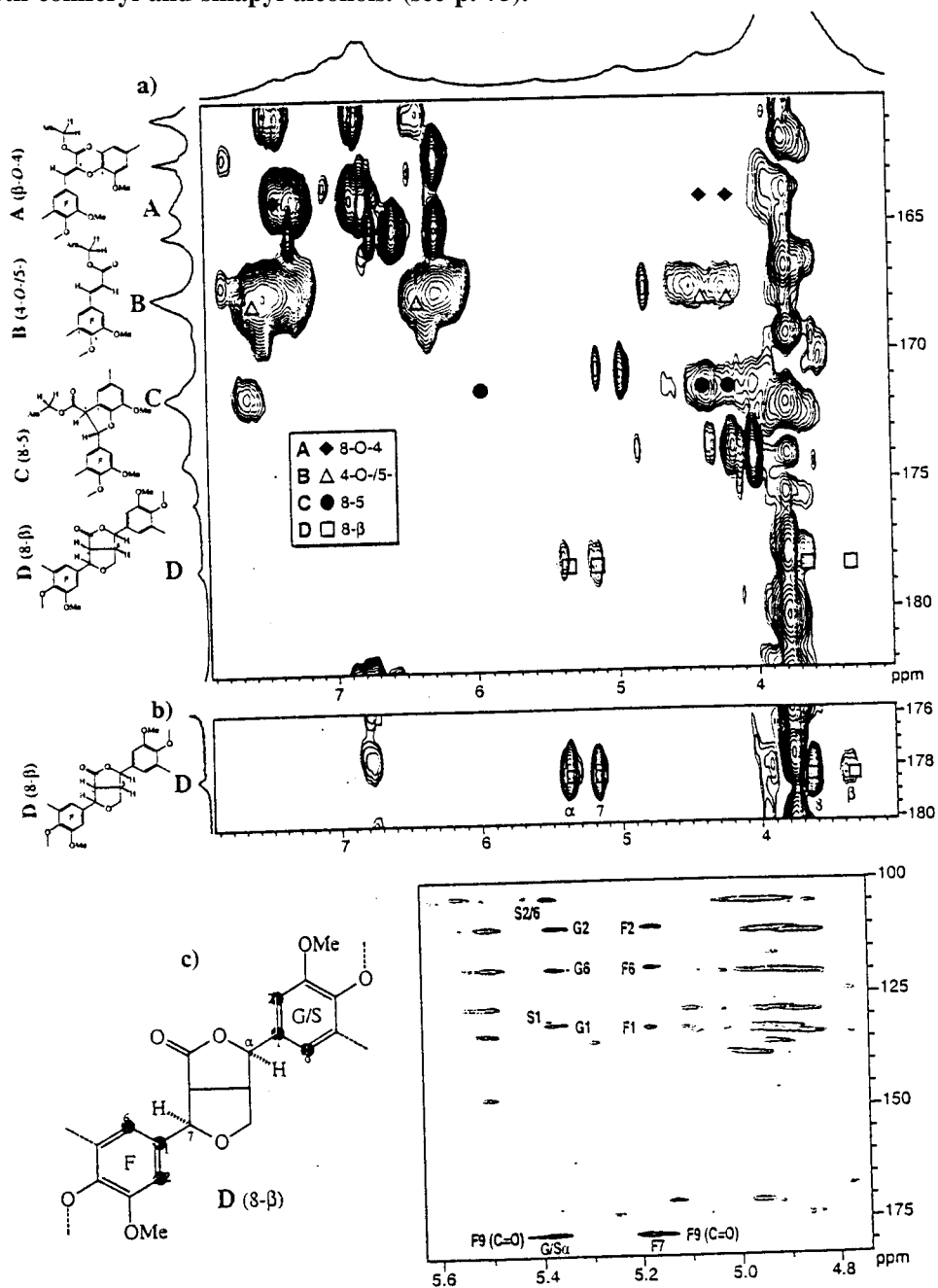
Figure 16: Sidechain region of 2D HMQC-TOCSY spectra of acetylated synthetic lignins prepared from *(E)*- and *(Z)*-coniferyl alcohols. (see p. 77).
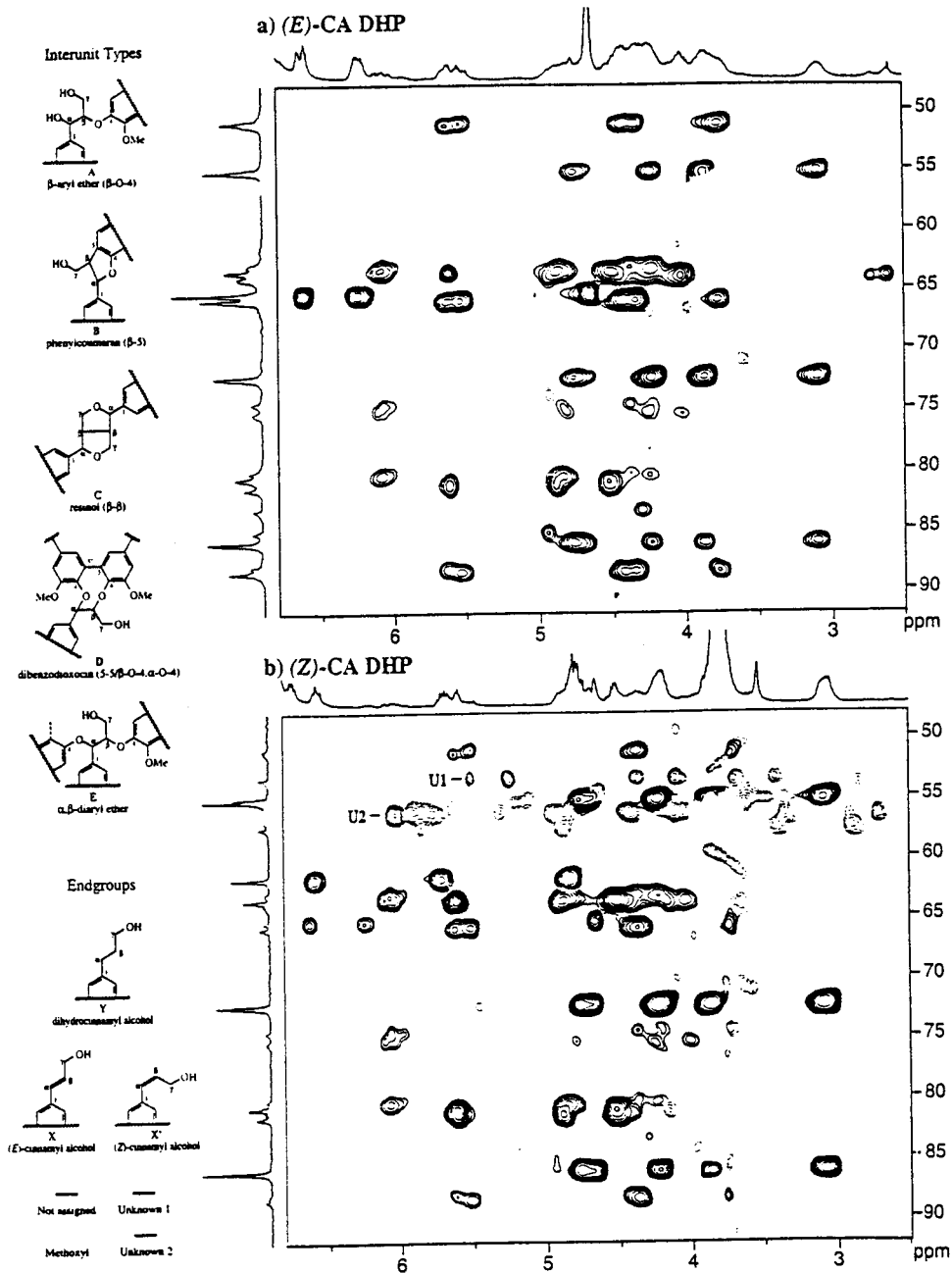
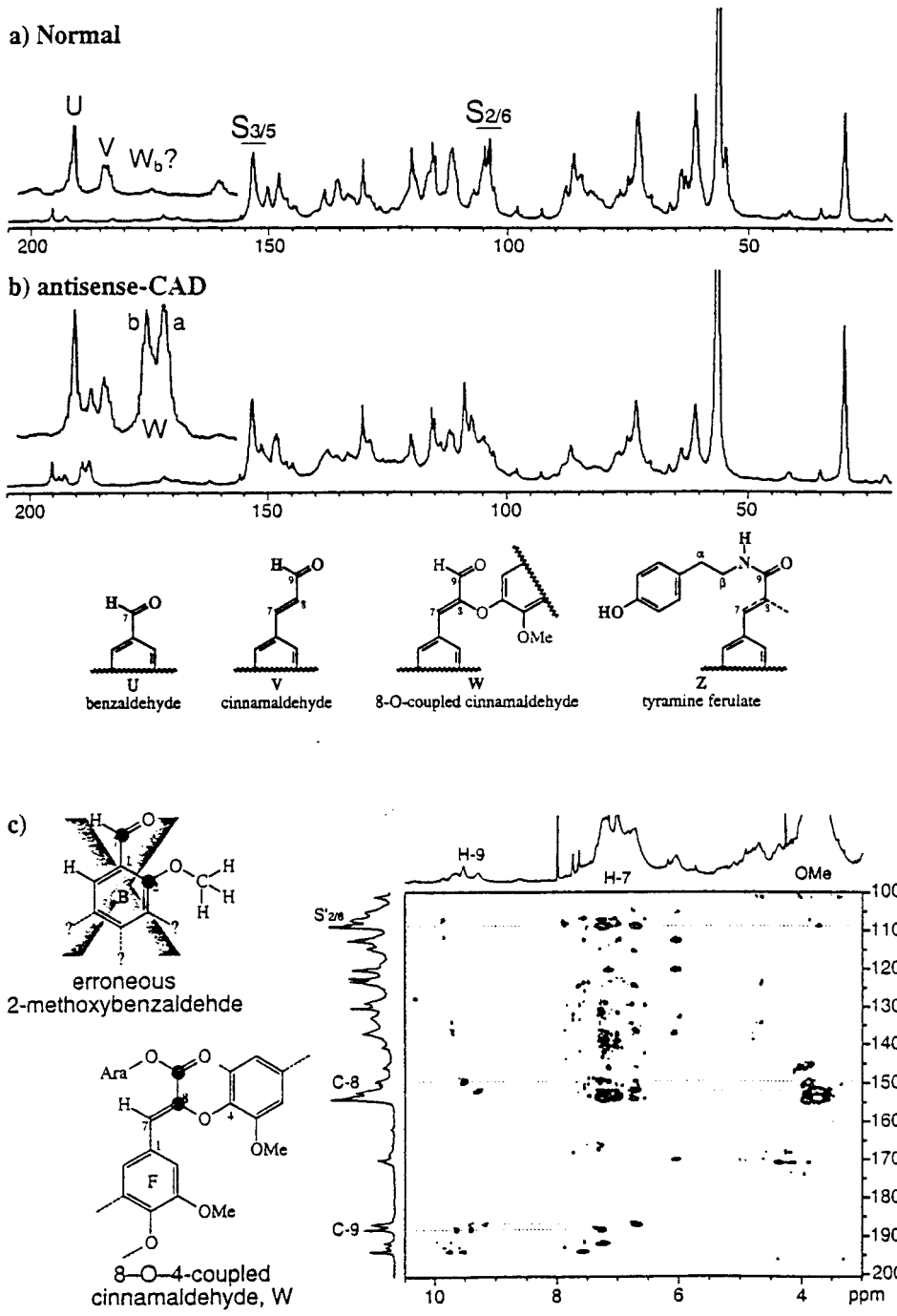## Figure 19: Spectra of normal and antisense-CAD tobacco isolated lignins. (see p. 80).

a) Normal

b) antisense-CAD

c)

erroneous
2-methoxybenzaldehde

8–O–4-coupled
cinnamaldehyde, W

100

Figure 20: Normal and CAD-deficient mutant pines and spectra of their isolated lignins (Seep. 81).
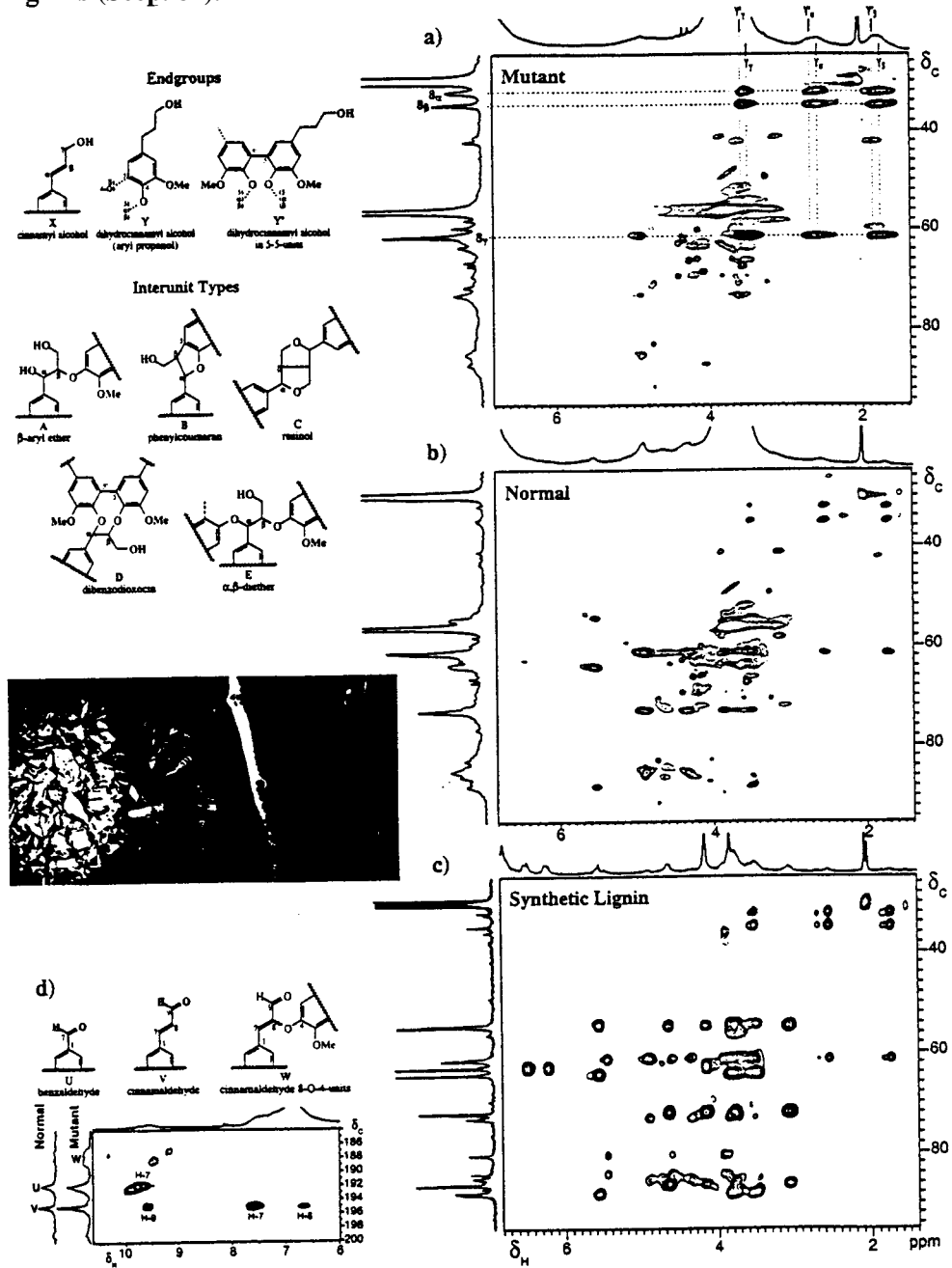
Figure 21: A closer look at the DHCA components Y that provide evidence for DHCA monomer incorporation—HSQC-TOCSY spectra. (see p. 82).

Figure 22: Diagnostic TOCSY spectra showing DHCA components Y in both a) the isolated lignin fraction and b) the entire residual lignin from CAD-deficient pine following dissolution and derivatization in propionyl bromide. (see p. 83).
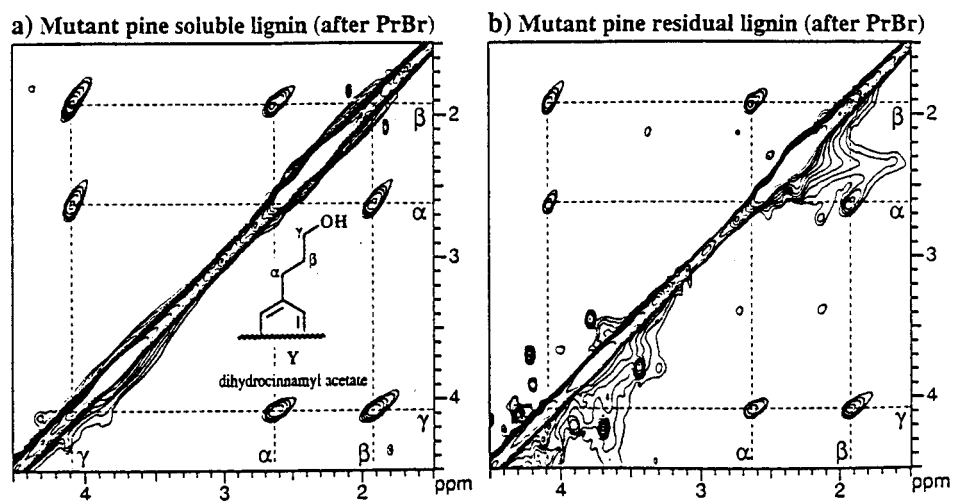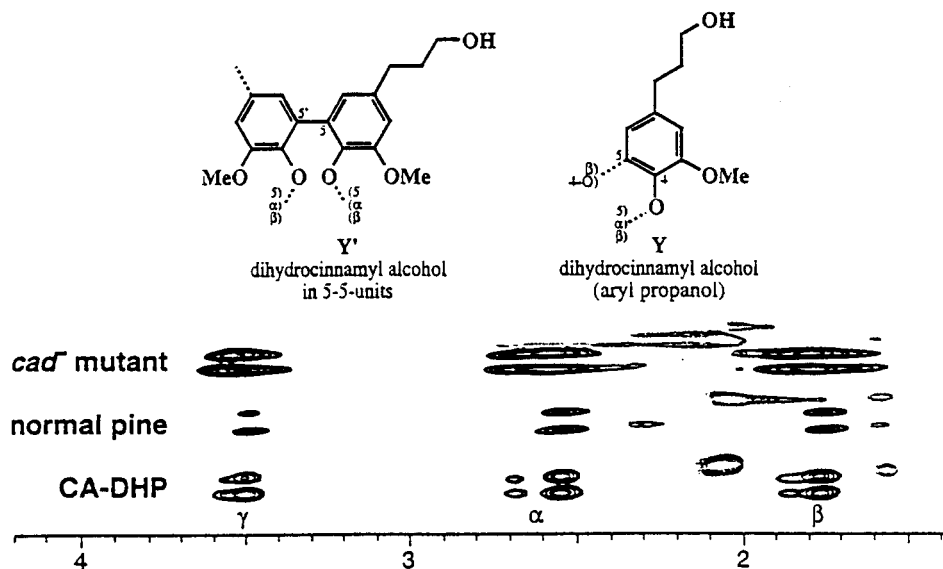
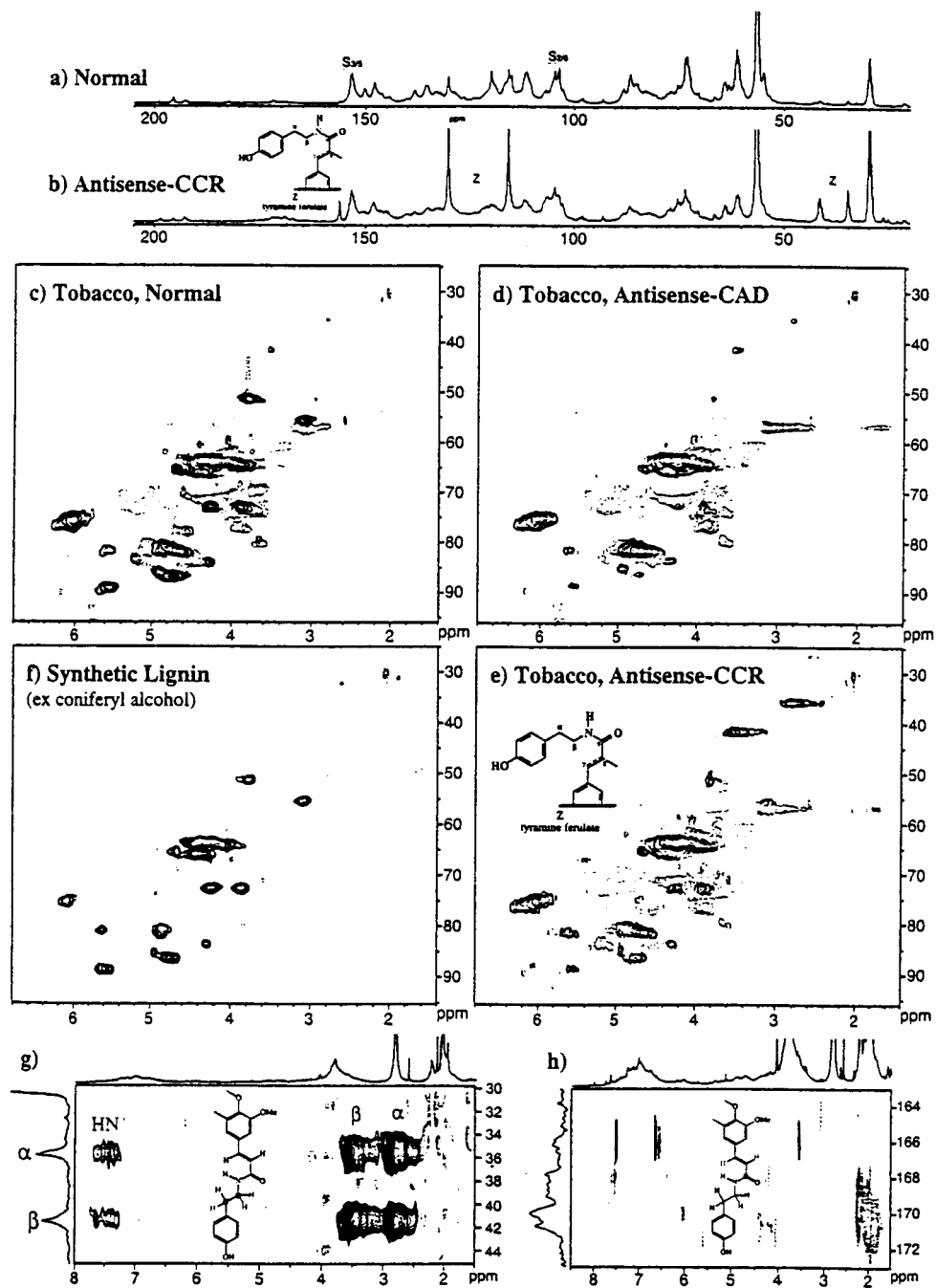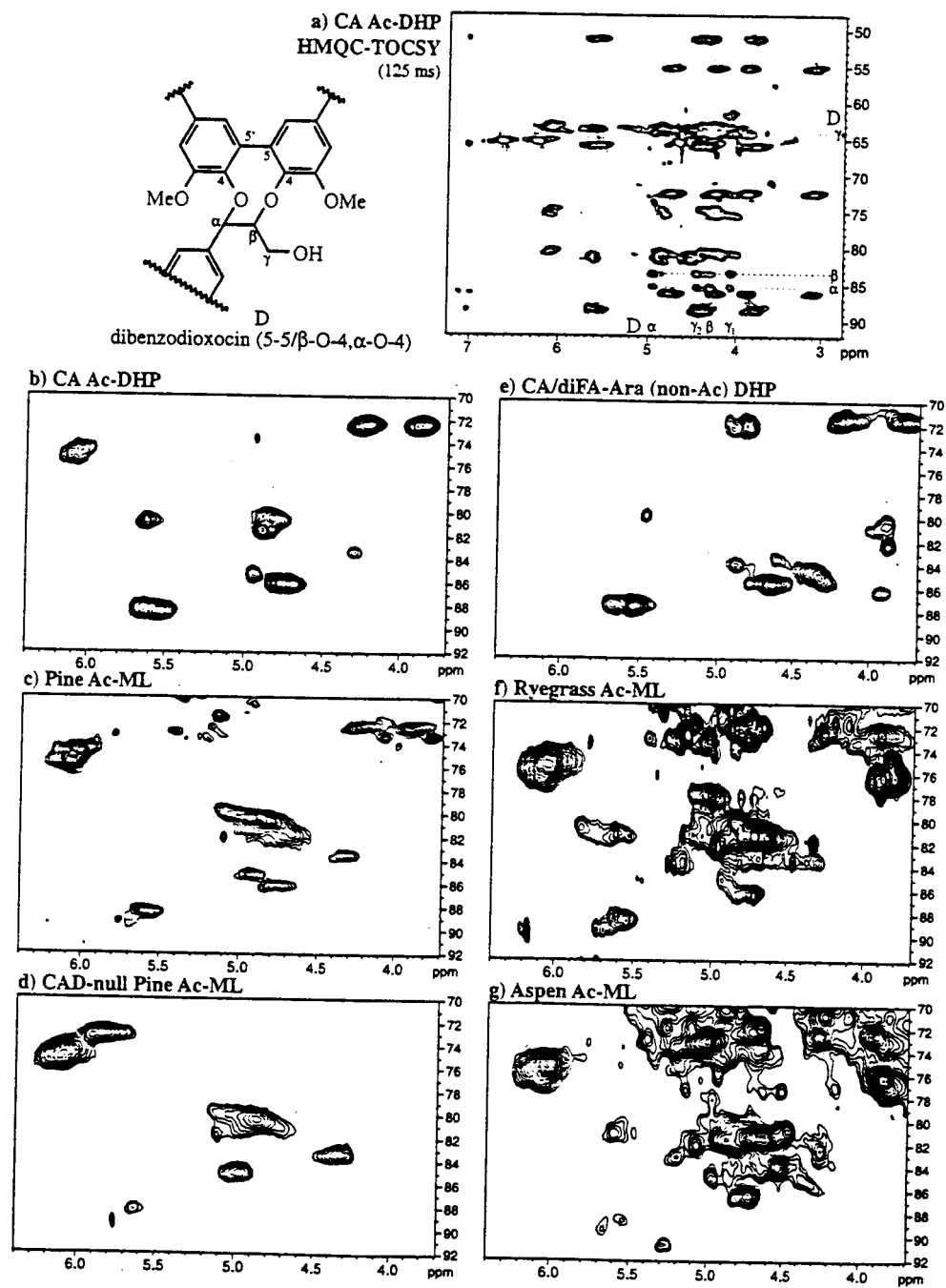**Figure 23: Spectra from tobacco normal and antisense-CAD and antisense-CCR lignins. (See p. 83).**

Figure 24: Spectra showing the dibenzodioxocins structure D in synthetic lignins and in isolated lignins from various plant classes. (see p. 84).

References

1. Lüdemann, H.-D., Nimz, H., *Makromol. Chem.* 175:2393 (1974).
2. Lüdemann, H.-D., Nimz, H., *Makromol. Chem.* 175:2409 (1974).
3. Kilpeläinen, I., Sipilä, J., Brunow, G., Lundquist, K., Ede, R.M., *J. Ag. Food Chem.* 42(12):2790 (1994).
4. Ede, R.M., Ralph, J., *Magn. Reson. Chem.* 34(4):261 (1996).
5. Ralph, J., *Magn. Reson. Chem.* 31(4):357 (1993).
6. Lundquist, K., Paterson, A., Ramsey, L., *Acta Chem. Scand.*, Ser. B B37(8):734 (1983).
7. Ralph, J., Rodger, C., NMR of Lignin Model Trimers, or why you will never find crystalline regions in lignin, Eds., Sixth International Symposium of Wood and Paper Chemistry (APPITA, Australia, Melbourne, Australia, 1991), Vol. 1, pp. 59.
8. Bax, A., Summers, M.F., *J. Am. Chem. Soc.* 108(8):2093 (1986).
9. Bax, A., Subramanian, S., J. *Magn. Reson.* 67(3):565 (1986).
10. Ralph, J., Zhang, Y., Ede, R.M., *J. Chem. Soc., Perkin Trans.* 1 (16):2609 (1998).
11. Kessler, H., Schmieder, P., Kurz, M., *J. Magn. Reson.* 85(2):400 (1989).
12. Lerner, L., Bax, A., *J. Magn. Reson.* 69(2):375 (1986).
13. Braun, S., Kalinowski, H.-O., Berger, S., *100 and More Basic NMR Experiments, a Practical Course.* Eds., VCH, New York, 1996).
14. Fukagawa, N., Meshitsuka, G., Ishizu, A., *J. Wood Chem. Technol.* 11(3):373 (1991).
15. Ede, R.M., Brunow, G., Simola, L.K., Lemmetyinen, J., *Holzforschung* 44(2):95 (1990).
16. Ede, R.M., Brunow, G., J. Org. Chem. 57(5):1477 (1992).
17. Ede, R.M., Ralph, J., Torr, K.M., Dawson, B.S.W., *Holzforschung* 50(2):161 (1996).
18. Fukagawa, N., Meshitsuka, G., Ishizu, A., *J. Wood Chem. Technol.* 12(4):425 (1992).
19. Fukagawa, N., Meshitsuka, G., Ishizu, A., *J. Wood Chem. Technol.* 12(1):91 (1992).
20. Quideau, S., Ralph, J., *Holzforschung* 48(2):124 (1994).
21. Ralph, J., Helm, R.F., Lignin/hydroxycinnamic acid/polysaccharide complexes: Synthetic models for regiochemical characterization, in *Forage Cell Wall Structure and Digestibility, International Symposium* (Jung, H.G., Buxton, D.R., Hatfield, R.D., Ralph, J., Eds.) ASA-CSSA-SSSA, Madison, WI, 1993), pp. 201.
22. Ralph, J., *J. Nat. Prod.* 59(4):341 (1996).
23. Ralph, J., MacKay, J.J., Hatfield, R.D., O'Malley, D.M., Whetten, R.W., Sederoff, R.R., *Science* 277:235 (1997).
24. Ralph, J., Zhang, Y., *Tetrahedron* 54:1349 (1998).

25. Ede, R.M., Kilpeläinen, I., *Res. Chem. Intermediates* 21(3-5):313 (1995).
26. Quideau, S., Ralph, J., *J. Chem. Soc., Perkin Trans.* 1 (6):653 (1993).
27. Kay, L.E., Keifer, P., Saarinen, T., *J. Am. Chem. Soc.* 114(26):10663 (1992).
28. Palmer, A.G., Cavanagh, J., Wright, P.E., Rance, M., *J. Magn. Reson. Ser. A* 93:151 (1991).
29. Davis, A.L., Keeler, J., Laue, E.D., Moskau, D., *J. Magn. Reson.* 98(1):207 (1992).
30. Ralph, S.A., Ralph, J., Landucci, W.L., Landucci, L.L., *Available over Internet at http://www.dfrc.ars.usda.gov/software.html.* (1996).
31. Quideau, S., Ralph, J., *J. Chem. Soc., Perkin Trans.* 1 (16):2351 (1997).
32. Ralph, J., Hatfield, R.D., Quideau, S., Helm, R.F., Grabber, J.H., Jung, H.-J.G., *J. Amer. Chem. Soc.* 116(21):9448 (1994).
33. Karhunen, P., Rummakko, P., Sipilä, J., Brunow, G., Kilpeläinen, I., *Tetrahedron Lett.* 36(1):169 (1995).
34. Karhunen, P., Rummakko, P., Sipilä, J., Brunow, G., Kilpeläinen, I., *Tetrahedron Lett.* 36(25):4501 (1995).
35. Karhunen, P., Rummakko, P., Pajunen, A., Brunow, G., *J. Chem. Soc., Perkin Trans.* 1 :2303 (1996).
36. Willker, W., Leibfritz, D., Kerssebaum, R., Bermel, W., *Magnetic Resonance in Chemistry* 31:287 (1992).
37. Ralph, J., Helm, R.F., Quideau, S., Hatfield, R.D., *J. Chem. Soc., Perkin Trans.* 1 :2961 (1992).
38. Ralph, J., Hatfield, R.D., Piquemal, J., Yahiaoui, N., Pean, M., Lapierre, C., Boudet, A.-M., *Proc. Nat. Acad. Sci.* 95:12803 (1998).
39. Ralph, J., Grabber, J.H., Hatfield, R.D., *Carbohydr. Res.* 275(1):167 (1995).
40. Bax, A., Freeman, R., Kempsell, S.P., *J. Am. Chem. Soc.* 102(14):4849 (1980).
41. Bax, A., Freeman, R., Frenkiel, T.A., *J. Am. Chem. Soc.* 103(8):2102 (1981).
42. Marcei, T.H., Freeman, R., *J. Magn. Reson.* 48(1):158 (1982).
43. Bardet, M., Gagnaire, D., Nardin, R., Robert, D., Vincendon, M., *Holzforschung* 40(Suppl.):17 (1986).
44. Guittet, E., Lallemand, J.Y., Lapierre, C., Monties, B., *Tetrahedron Lett.* 26(22):2671 (1985).
45. Lapierre, C., Monties, B., Guittet, E., Lallemand, J.Y., *Holzforschung* 41(1):51 (1987).
46. Lapierre, C., Gaudillere, J.P., Monties, B., Guittet, E., Rolando, C., Lallemand, J.Y., *Holzforschung* 37(5):217 (1983).
47. Kilpelainen, I., Ammalahti, E., Brunow, G., Robert, D., *Tetrahedron Lett.* 35(49):9267 (1994).
48. Ammalahti, E., Brunow, G., Bardet, M., Robert, D., Kilpelainen, I., *J. Agric. Food Chem.* 46(12):5113 (1998).

49. Bigler, P., NMR *Spectroscopy: Processing Strategies*. Eds., VCH, Weinheim, Germany, 1997).
50. Hoch, J., Stern, A.S., *NMR Data Processing*. Eds., Wiley, New York, N. Y., 1996), Vol. .
51. Pelczer, I., Szalma, S., *Chemical Reviews* 91(7):1507 (1991).
52. Sarkanen, K.V., Chang, H.-M., Allan, G.G., *Tappi* 50(12):587 (1967).
53. Smith, D.C.C., *Nature* 176:267 (1955).
54. Scalbert, A., Monties, B., Lallemand, J.Y., Guittet, E., Rolando, C., *Phytochemistry* 24(6):1359 (1985).
55. Shimada, M., Fukuzuka, T., Higuchi, T., *Tappi* 54(1):72 (1971).
56. Monties, B., Lapierre, C., *Physiologie Végétale* 19(3):327 (1981).
57. Atsushi, K., Azuma, J., Koshijima, T., *Holzforschung* 38(3):141 (1984).
58. Azuma, J., Nomura, T., Koshijima, T., *Agric. Biol. Chem.* 49:2661 (1985).
59. Terashima, N., Fukushima, K., He, L.-F., Takabe, K., Comprehensive model of the lignified plant cell wall, in *Forage Cell Wall Structure and Digestibility* (Jung, H.G., Buxton, D.R., Hatfield, R.D., Ralph, J., Eds.) ASA-CSSA-SSSA, Madison, 1993), pp. 247.
60. Lam, T.B.T., Iiyama, K., Stone, B.A., *Phytochemistry* 31(8):2655 (1992).
61. Nakamura, Y., Higuchi, T., *Cellul. Chem. Technol.* 12(2):199 (1978).
62. Landucci, L.L., Deka, G.C., Roy, D.N., *Holzforschung* 46(6):505 (1992).
63. Kratzl, K., Okabe, *Tappi* 48:347 (1965).
64. Ralph, J., Lu, F., *J. Agric. Food Chem.* 46(11):4616 (1998).
65. Helm, R.F., Ralph, J., *J. Wood Chem. Tech.* 13(4):593 (1993).
66. Takahama, U., Oniki, T., *Plant Cell Physiol.* 35(4):593 (1994).
67. Takahama, U., Oniki, T., Shimokawa, H., *Plant Cell Physiol.* 37(4):499 (1996).
68. Hatfield, R.D., Grabber, J.H., Ralph, J., *Plant Physiology* :in preparation (1998).
69. Nakamura, Y., Higuchi, T., *Holzforschung* 30(6):187 (1976).
70. Helm, R.F., Ralph, J., *J. Agric. Food Chem.* 41(4):570 (1993).
71. Crestini, C., Argyropoulos, D.S., *J. Agric. Food Chem.* 45(4):1212 (1997).
72. Ralph, J., Hatfield, R.D., Grabber, J.H., Jung, H.G., Quideau, S., Helm, R.F., Cell wall cross-linking in grasses by ferulates and diferulates, in *Lignin and Lignan Biosynthesis* (Lewis, N.G., Sarkanen, S., Eds.) American Chemical Society, Washington, DC, 1998), ACS Symposium Series, No 697, pp. 209.
73. Ralph, J., Quideau, S., Grabber, J.H., Hatfield, R.D., *J. Chem. Soc., Perkin Trans.* 1 (23):3485 (1994).
74. Grabber, J.H., Ralph, J., Hatfield, R.D., Quideau, S., Kuster, T., Pell, A.N., *J. Agric. Food Chem.* 44(6):1453 (1996).
75. Lam, T.B.T., Iiyama, K., Stone, B.A., *Phytochemistry* 31:1179 (1992).
76. Lam, T.B.T., Iiyama, K., Stone, B.A., *Phytochemistry* 36(3):773 (1994).
77. Helm, R.F., Ralph, J., *J. Agric. Food Chem.* 40(11):2167 (1992).
78. Hatfield, R.D., Helm, R.F., Ralph, J., *Anal. Biochem.* 194(1):25 (1991).

79. Jacquet, G., Pollet, B., Lapierre, C., Mhamdi, F., Rolando, C., *J. Agric. Food Chem.* 43(10):2746 (1995).

80. Terashima, N., Fukushima, K., Tsuchiya, S., Takabe, K., *J. Wood Chem. Technol.* 6(4):495 (1986).

81. Terashima, N., Fukushima, K., Takabe, K., *Holzforschung* 40(Suppl.):101 (1986).

82. Morelli, E., Rej, R.N., Lewis, N.G., Just, G., Towers, G.H.N., *Phytochemistry* 25(7):1701 (1986).

83. Boudet, A.-M., *Trends in Plant Science* 3(2):67 (1998).

84. Lewis, N.G., Lignins, lignans and abnormal lignins: a biochemical clarification, 215th Amer. Chem. Soc. Natl Mtg. (Amer. Chem. Soc., Dallas, TX, 1998), Vol. 1, pp. Cell 09.

85. Meyer, K., Shirley, A.M., Cusumano, J.C., Bell-Lelong, D.A., Chapple, C., *Proc. Natl. Acad. Sci.* USA 95(12):6619 (1998).

86. Yahiaoui, N., Marque, C., Myton, K.E., Negrel, J., Boudet, A.-M., *Planta* 204(1):8 (1998).

87. MacKay, J.J., O'Malley, D.M., Presnell, T., Booker, F.L., Campbell, M.M., Whetten, R.W., Sederoff, R.R., *Proc. Natl. Acad. Sci. U. S. A.* 94(15):8255 (1997).

88. Gang, D.R., Fujita, M., Davin, L.D., Lewis, N.G., The 'abnormal lignins': mapping heartwood formation through the lignan biosynthetic pathway, in *Lignin and Lignan Biosynthesis* (Lewis, N.G., Sarkanen, S., Eds.) Amer. Chem. Soc., Washington, DC, 1998), ACS Symposium Series 697, pp. 389.

89. Ralph, J., Recent advances in characterizing 'non-traditional' lignins and lignin-polysaccharide cross-linking, 9th International Symposium on Wood and Pulping Chemistry (CPPA (Canadian Pulp and Paper Association), Montreal, Quebec, 1997), Vol. 1, pp. PL2 (1).

90. Ralph, J., Lu, F., Kim, H., MacKay, J.J., Sederoff, R.R., *J. Agric. Food Chem.*, in preparation (1999).

91. Piquemal, J., Lapierre, C., Myton, K., O'Connell, A., Schuch, W., Grima-Pettenati, J., Boudet, A.-M., *Plant J.* 13(1):71 (1998).

92. Bernards, M.A., Lewis, N.G., *Phytochem.* 47(6):915 (1998).

93. Galkin, S., Ämmälahti, E., Kilpeläinen, I., Brunow, G., Hatakka, A., *Holzforschung* 51(2):130 (1997).

94. Peng, J., Lu, F., Ralph, J., *Phytochem.* 50(4):659 (1998).

95. Ralph, J., Peng, J., Lu, F., *Tetrahedron Lett.* 39(28):4963 (1998).